CHARACTERIZATION OF IMMUNE RESPONSE AND PERIPHERAL NERVE REGENERATION OF IMPLANTED REGENERATIVE MULTI-ELECTRODE INTERFACE POST-SUBCHRONIC AMPUTATION

by

CAMILO ANDRES SANCHEZ USECHE

Presented to the Faculty of the Graduate School of

The University of Texas at Arlington in Partial Fulfillment

of the Requirements

for the Degree of

MASTERS OF SCIENCE IN BIOMEDICAL ENGINEERING

THEUNIVERSITY OF TEXAS AT ARLINGTON

December 2012

Acknowledgements

I want to thank my father, mother, and grandmother, Gustavo Sanchez, Liliana Useche, and Argelia Martinez, respectively. The upbringing and support they have provided to me are the reasons why I am presenting this thesis today. Also, I want to thank Belle Marco for her support and for being the most influential motivator throughout my college career.

I am thankful to Dr. Romero for believing in me and giving me the opportunity to work in a prosthetics-related project; also, for the time and resources he dedicated to me. The dedication he applies to his job has truly been an inspiration to me.

I appreciate Dr. Hong and Dr. Tang for being part of my committee; their suggestions for my thesis gave me different and helpful perspectives. Also, I want to thank Dr. Kim for his help and input on my project.

Finally, I want to take time to recognize being part of a helpful and knowledgeable laboratory; from undergraduates all the way to the post-doctoral students--they kindly assisted me whenever I needed it.

November 28, 2012

Abstract

CHARACTERIZATION OF IMMUNE RESPONSE AND PERIPHERAL NERVE REGENRATION OF IMPLANTED REGENERATIVE MULTI-ELECTRODE ARRAY POST-SUBCHRONIC AMPUTATION

Camilo A. Sanchez U., Masters Student

The University of Texas at Arlington, 2012

Supervising Professor: Mario Ignacio Romero Ortega

Interfacing high degree-of-freedom robotic prosthetics directly to the peripheral nervous system aims at improving the quotidian life of amputees. Despite advancements in robotics that have lead to human-like upper limb prosthetics, long-term interfacing has not been accomplished, thus voiding them from clinical use. Interfacing electrodes in the central nervous system fail due to the foreign body reaction and glial scar formation at the site of implantation. Concrete mechanisms for the failure of long-term Interfacing at the peripheral nervous level remain unclear. A regenerative multi-electrode interface (REMI) which allows for action potential recording as early as 7 days and provides support to bridge transected nerve gaps has been recently tested. However, the REMI, similarly to other electrode arrays, suffers from decay in action potential signal acquisition after an extended period of time. Patients require between 6 to weeks for stabilization after amputation; therefore, the effects of a subchronic amputation must be studied to evaluate the peripheral nerve reaction to interfacing. A 30-day subchronic amputation condition was performed by transecting the sciatic nerve, ligating the distal stump, and suturing the proximal stump to the biceps femoris muscle of twelve female adult Lewis rats. Floating multi-electrode arrays comprising 18 Pt/Ir

electrodes, placed in collagen-filled Polyurethane tubes, were implanted after subchronic amputation in the animals by suturing the stumps of transected sciatic nerve to the tube. The REMI , along with the nerve regenerate, was explanted after 15, 30, and 60 days. Reactive macrophages, visualized by immunofluorescence of ED1 labeling, showed a significant reduction in size between 15 and 60 days post REMI implantation for acute and subchronic amputation conditions. The progressive decreasing pattern indicates that scar formation around the electrodes does not directly affect the action potential signal acquisition; regardless, it may still play a minor role in interfacing failure. Axonal regeneration and remyelination were examined by immunolabeling with NF200 and P0, respectively. Axonal regeneration and remyelination between subchronic and acute amputation conditions revealed comparable patterns qualitatively but not quantitatively at 30 and 60 days post REMI implantation. The complete remyelination of the axons directly correlates with the maximum percentage of active channels; however, it does not account for the eventual signal decay. Blood nerve barrier integrity was evaluated to determine whether tight junction formation and/or distribution of perineurial cell had an effect on ion diffusion in the extracellular matrix. Through the use of anti-Claudin-1 antibodies, a progressive distribution and organization of tight junctions around and through the axons was observed for acute and subchronic amputation conditions. Foreign body response and BNB formation results indicate that a subchronic amputation does not significantly affect these mechanisms when compared to the acute amputation conditions; however, axon regrowth and axon remyelination extent were significantly less for the subchronic model than the acute model. Further, it is hypothesized formation of the BNB around the implanted interfacing electrodes plays an important role in the eventual failure of peripheral nerve interfacing.

Table of Contents

List of Illustrations

Chapter 1

Introduction

Motivation

Approximately 1.8 million individuals in the United States were estimated to have lost a limb by 2010; over 3.6 million people are expected to lose limb by 2050 (Ziegler-Graham, MacKenzie et al. 2008; Resnik, Meucci et al. 2012). Amputees face psychological, emotional, and physical challenges which vary from acceptances self-body image acceptances, to physical impairment, to chronic pain (Karami, Ahmadi et al. 2012). Despite the fact that prosthetics have been used to rehabilitate affected individuals for over 3500 years (Cochrane et al. 2001), current devices are incapable of approaching the complexity level or reliability of the natural limb it is designed to replace. Exoskeletons and robotic prosthetics, which hold promise for amputees, are mainly limited by the lack of user control (Bogue 2009). Robotic prosthetics posses the potential to be controlled by either central nervous or the peripheral nervous system interfacing; the modality of which usually positively correlates selectiveness to invasiveness (Kim and Romero-Ortega 2012). The most selective interfaces correlate with the most invasive methods of signal acquisitions. The perplexity of these invasive brain-computer and peripheral interfaces originate from the signal acquisition decay over time. Previous studies performed in our laboratory have shown that micromotion or immune response of acutely implanted regenerative multi-electrode arrays (REMIs) are not a cause of signal acquisition decay (Khobragade, 2011). Most amputees today have not been interfaced, thus categorizing them as non-acute amputation candidates for potential neural interfacing. This study aims to further understand signal acquisition decay under subchronic implantation of the REMI.

Etiology of Amputation

In 2010, approximately 55% of amputations the United States were due to dysvascular disease. Trauma accounted for about 44% of individuals who suffered from limb loss, while cancer ranked 3rd with 1%. (Ziegler-Graham, MacKenzie et al. 2008). Most trauma-caused amputations are of the upper limb, while dysvascular disease accounts for 80% of amputations of the lower limb (Resnik, Meucci et al. 2012). 60% of diabetes type II patients suffered from amputations, mainly due to foot ulcers, which is the result of a combination of peripheral vascular disease, neuropathy, infection, and inadequate foot care (Viswanathan and Kumpatla 2011). Amputation etiology is

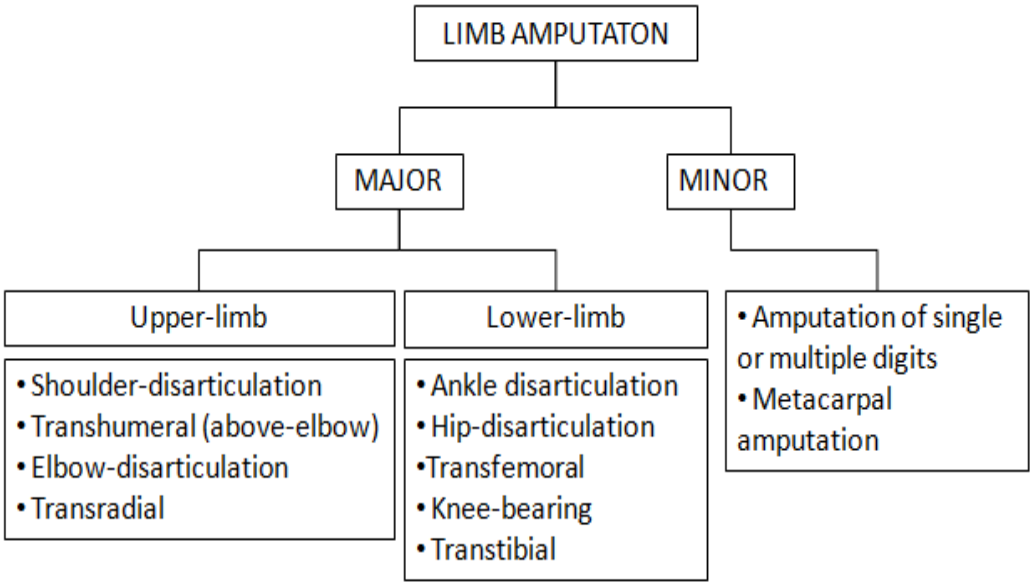

Figure 1-1 Classification of major and minor limb amputations (Adapted from Nivedita, 2011)

distributed differently internationally due to different poverty and war conditions (Weir, Ephraim et al. 2010). The Afghanistan and Iraq Wars have been a major factor in the increase of traumatic amputations, mainly by the use of improvised explosive devices

(IED) (Resnik, Meucci et al. 2012). Figure 1-1 offers more detail about major and minor amputation categorization.

Nervous System Interfacing

For over half a century the interest and ability in interfacing human with machines has increased, partly due to the available technology which is constantly being developed (Coates 2008). Direct control of machines by the nervous system aim at (1) the replacement of damaged central motor units; (2) using interfaces to control robotic prosthetics of missing limbs; (3) controlling exoskeletons for the augmentation or restoration of body movements; (4) tele-operation of robots to accomplish tasks (Navarro, Krueger et al. 2005). Since the creation of the transistor, computers have become exponentially faster and smaller (Taylor, Cunningham et al. 1999; Ismagilov 2003), which has allowed scientists to envision the idea of permanently implanting electrodes at the nervous system level with the ultimate intentions to control a machine. Cortical interfacing has been a subject of speculation among the scientific community since the first EEG was accomplished by Hans Berger in 1929 (Shoham 2001). Brain-computer interfaces (BNI) promised an increase in quality of life not only to paraplegics and quadriplegics, but also to people suffering from amyotrophic lateral sclerosis, brainstem stroke, and cerebral palsy (Vaughan 2003). Concurrent to the idea of cortical interfaces, peripherally interfacing a subject to gain control of a machine was a logical step to follow. Interfacing of the peripheral nervous system to robotic prosthetics possesses the potential to replace lost limbs of amputees without invasive procedures in the brain, making this a lucrative option for amputees and potentially paraplegics. Figure 1-2 summarizes some of the major differences between CNS and PNS interfacing.

Differences	Brain	Peripheral Nerve
Cells involved in inflammatory response and scar tissue	Microglia, astrocytes, and meninges-derived fibroblasts	Macrophages, Schwann cells, and fibroblasts
AP source	Neuronal cell bodies and myelinated/unmyelinated axons	Myelinated/unmyelinated axons
Presence of neural cell body	Yes. Neuronal cell bodies are located close to electrode	No. Motor and sensory neuronal cell bodies are located at the spinal cord and DRG, respectively
AP specificity to target limb	Recorded APs may not be exclusive for target limb	Recorded APs are exclusively for target limb
Similarity	**Brain**	**Peripheral Nerve**
Scar tissue formation at implanted electrode	Implanted electrode is encapsulated by inflammatory/scar tissue	
Scar tissue effect on function of electrode	Function of implanted electrode is influenced by severity of scar tissue	

Figure 1-2 Differences between central nervous and peripheral nervous interfacing (adapted from (Kim and Romero-Ortega 2012))

Central Nervous Interfacing

Current electroencephalographic activity (EEG) technology provides the least invasive method in which information can be relayed from the CNS to a machine, otherwise known as a Brain-machine interface (BMI). Electrocorticographic activity (ECoG) recorded from the brain cortex provides more selectivity for control, but requires surgical procedure and hence it is more invasive. Intracortical activity is more invasive than ECoG methods because the electrode arrays penetrate the brain cortex; however, this method has proven to be one of the most promising for CNS interfacing (Velliste, Perel et al. 2008; McFarland, Sarnacki et al. 2010). ECoG and intracortical signal acquisition and stimulation both require invasive craniotomy surgery, making BMI via ECoG or intracortical interfacing appealing to extreme disabled subjects such as quadriplegics awhile turning away subjects with less severe cases such as single and double amputees. Moreover, lack of sensory discrimination and modulation from other

regions in the CNS required for context-dependant control limit the use of BMIs (Brown, Koerber et al. 2004; Lee, Carvell et al. 2008).

Peripheral Nervous Interfacing

Interfacing the nervous system at the peripheral level is generally more invasive than EEG interfacing methods because the electrodes need to be in direct contact with the nerve. In general, PNS interfacing requires minor operation in relation to the more invasive craniotomy surgery required for most BMIs. In terms of prosthetic control, PNS interfacing has not yet been proven to be significantly advantageous over CNS interfacing for controlling robotic prosthesis due to lower amount of degrees of freedom (DOF) which is able to operate (Watson 2012). However, interfacing the PNS offers a readily accessible gate to the bidirectional information flow between the nervous system of the subject and the robotic prosthetic, i.e., sensory feedback from the prosthetic and motor control of the prosthetic (Kim and Romero-Ortega 2012). Thus, Peripheral nerve interfacing, with its less invasive required surgeries than most BMI methods and its potential to create a bidirectional flow of information between user and prosthetic, presents itself as an ideal solution to improving the quality of life of amputees. Figure 1-3 demonstrates the concept of invasiveness and selectivity.

Over the past few decades research on PNS interfacing has lead to the creation of many types of electrodes through the use of different materials and designs. Breakthroughs in material science have aided in the development of better interfacing electrodes. Biocompatibility and corrosion resistance in electrodes for action potential recording and nerve stimulation have been made possible through the use of gold, titanium, tungsten, platinum, iridium oxide, stainless steel, semiconductors and conductive polymers (Merrill, Bikson et al. 2005). Peripheral interfacing electrode designs have always compromised between two characteristics: selectivity and

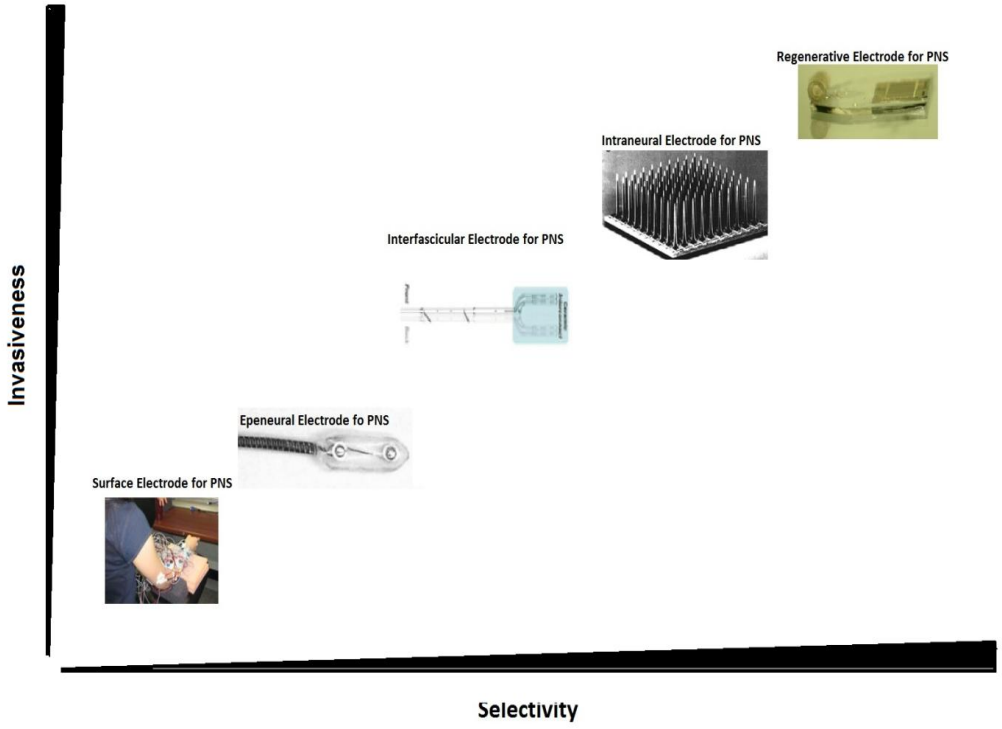

Figure 1-3 Invasiveness versus selectivity. As invasiveness increases, the selectivity of the interfacing electrode also increases (and vice versa)

invasiveness (Navarro, Krueger et al. 2005; Kim and Romero-Ortega 2012). A direct relationship between sensitivity and invasiveness exists; the more selective that an interfacing electrode is desired, the more invasive its design will be. The implantation of such invasive interfacing electrodes can be justified in most amputees because the nerve in the limb stump remains functional in terms of signal transduction but has lost its previous function of limb control. Also, as previously mentioned, interfacing of the peripheral nerve for single and double amputees seems more advantageous in regards to the risks and rewards encountered through CNS interfacing. Throughout the past few decades, several designs for electrode interfaces with a wide variety of drawbacks and advantages have been designed—from low to high invasiveness as well as low to high selectivity—all which aim at exploiting the anatomy of the peripheral, shown in figure 1-4.

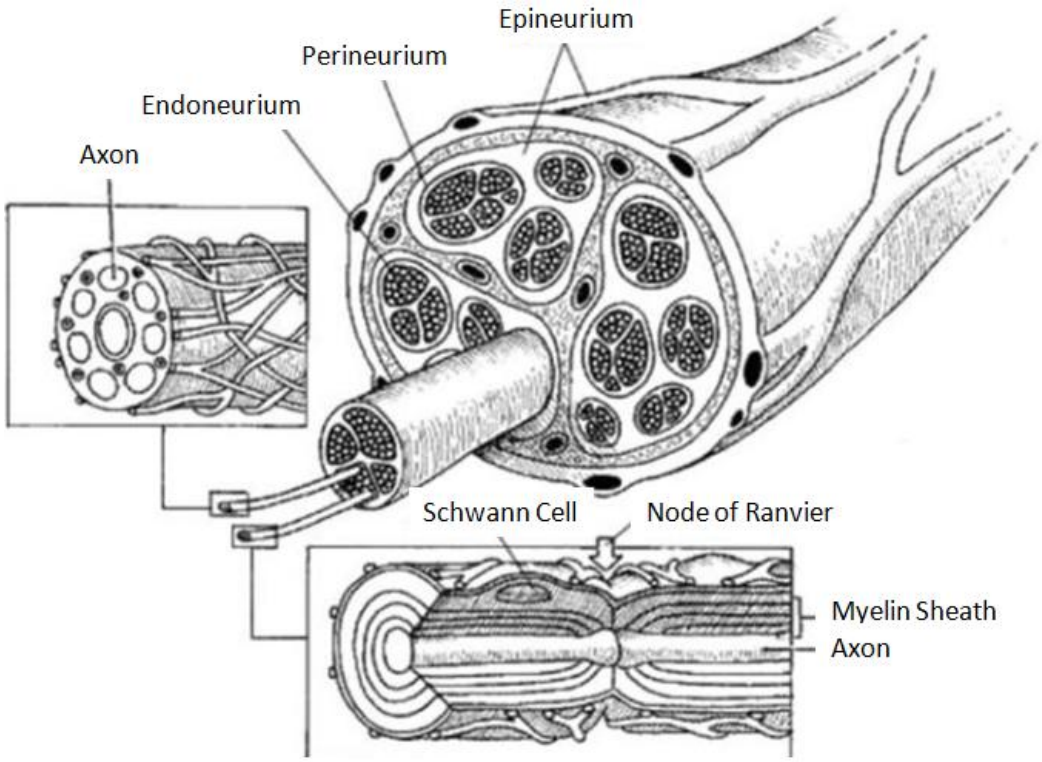

Figure 1-4 Peripheral nerve anatomy. As the interfacing electrode becomes more invasive it penetrates through the different layers (epineurium, perineurium, and endoneurium) thus decreasing the distance and barriers between the electrode itself and the action potential signals from the axons (A.D.A.M Anatomy 2009)

Surface Electrodes

Surface electrodes allow for the only noninvasive method to acquire neuromuscular signals. These electrodes are simply placed on the skin at key points of the body to in order to reach interfacing. Their simplicity to set up and maintain make surface electrodes a prime candidate method to control simple robotic arms—not high DOF prosthetics. Surface electrodes rely on surface EMG (sEMG) technology to acquire depolarization and repolarization signals from muscle fibers and peripheral nerves (Navarro, Krueger et al. 2005). Recent attempts to improve sEMG in terms of selectivity

with the aim to control prosthetics with higher DOF have sacrificed the noninvasiveness of the sEMG electrodes. Targeted muscle reinnervation surgery consists of denerverating the pectoralis muscle and reinnervating the same muscle with nerves that originally targeted the missing limb. This allows for the electromyography signal sites to increase in density and thus improve the controlled movement of a 6 DOF robotic arm. Targeted muscle reinnervation combined with sEMG has produced the best results in humans at a clinical level to this day; however, approximately a two-year window exists between the targeted muscle reinnervation surgery and the fitting of the robotic prosthetic. Surface electrodes are impermanent, which forces the subjects to frequently place and calibrate the electrodes (Navarro, Krueger et al. 2005; Miller, Lipschutz et al. 2008; Watson 2012).

Extraneural Electrodes

Epineural electrodes have been utilized for over 50 years to achieve controllable, progressive muscle contraction and reduce muscle fatigue during functional electrostimulation (Liberson WT 1961; Thoma, Girsch et al. 1989). They can be made of various metals such as platinum or platinum-iridium allow wires, which make direct contact with the nerve and are secured via microsurgery techniques to the epineurium. In terms of nerve invasiveness, epineural electrodes rank among the lowest because generally the nerve trunk remains intact; albeit, the securing sutures can potentially create tension forces capable of damaging the integrity of the epineurium and result in the disengagement of the electrodes to from the nerve. Helicoidal variations of the epineural electrode have been shown to decrease the amount of tension placed on the nerve due to their flexible material composition and structural design, thus diminishing the possibilities of nerve trauma (Navarro, Krueger et al. 2005). Cuff electrodes have been used for decades and have been proven to provide advantages such as noninvasiveness; moreover, extensive information about this design exists due to their

widespread use in the research field. Human trials have shown their capability of maintaining a consistent stimulation charge threshold, which is necessary to elicit a significant degree of muscle stimulation, 63 weeks post-implantation (Fisher, Tyler et al. 2009). Generally, cuff electrodes are limited to the recording of compound action potentials (CAPs); i.e., selective information about axons cannot be accessed (Branner and Normann 2000). The basic design of cuff electrodes are cylindrical shaped insulating material housing electrodes in the inner walls which wraps around the nerve. Cuff electrodes allow for multiple opportunities of their correct placement on the nerve thus preventing mechanical distortion and lead failure (Loeb and Peck 1996; Kim and Romero-Ortega 2012). Advances in biomaterials, specifically those applicable in the field of neural interfaces, have allowed for the miniaturization of the cuff electrode in the past decade. Smaller cuff electrodes have the potential of transforming such electrodes from extraneural to intraneural by allowing the cuffs to wrap around individual nerve fascicles and increase the selectivity of stimulated muscles (Stieglitz, Beutel et al. 2000; Navarro, Krueger et al. 2005). Alterations to the basic design of the cuff electrodes have led to the creation of flat interface nerve electrode (FINE). FINEs allow for more selective neural readings and stimulations because their structure forces the peripheral to flatten, allowing the inner fascicles to approach the epineurium to improve signal acquisition, i.e., the flattening of the nerve brings the inner fascicles into closer proximity with the electrodes of the nerves (Durand, Park et al. 2009). In regards to the structure design epineural electrodes have reached their potential; future improvements to this pioneering electrode are left to new material fabrications and coating enhancements, as will be discussed under Electrode Enhancements section.

Interfascicular Electrodes

Interfascicular electrodes aim at achieving comparable results as intraneural electrodes without compromising the integrity of perineurium. The basic design of

interfascicular electrodes is similar to those of penetrative intraneural electrodes. These electrodes will bluntly insert themselves within the nerve by perforating through the epineurium and positioning the electrodes within the different nerve fascicles which a cuff electrode would not be able to reach (Taylor, Cunningham et al. 1999; Navarro, Krueger et al. 2005). Attempts in the 1980s to achieve interfascicular stimulation through the use of nylon-coated and coiled stainless steel wires as electrodes resulted in inconclusive results. The coiled wired intraneural electrode (CWIE) did not show any significant advantage over previous interfacing electrodes; furthermore, the surgery required for implantation was rather complex in comparison to current methods at the time (Bowman and Erickson 1985). The slowly penetrating interfascicular nerve electrode (SPINE) was designed by Tyler et al., to test the advantage of obtaining interfascicular neural stimulation as opposed to extraneural electrodes. This design consists of a couple cylindrical structures that wrap around the peripheral nerve; the larger cylindrical tube has a frayed end with platinum beams which slowly insert them through the epineurium and position themselves among the nerve fascicles. The insertion of four-beam SPINEs showed that spacing as minute as 0.5 mm in depth were selective in 68% of the trials, while the opposing beams were selective in 90% of the trials (Tyler and Durand 1997). Longitudinal intrafasciular electrodes fabricated from Teflon-coated wire(PtIrLIFEs) allow for selective neural signal acquisition and stimulation due to their topology for a more discrete control and natural feedback of robotic prosthesis (Goodall and Horch 1992; McNaughton and Horch 1996). Also, PtIrLIFEs have demonstrated their capacity for long term implantation (up to six months in felines) despite a reduction in the signal-to-noise rations attributed to differential motion of the electrode within the fascicles (Goodall, Lefurge et al. 1991; Lefurge, Goodall et al. 1991). To address the mechanical mismatch in previous metal LIFEs, a Kevlar based LIFE insulated with medical-grade silicone was created (polyLIFE). The polyLIFE is 60 times more flexible than the PtIrLIFE and posses a higher degree of

biocompatibility with a reduction in differential motion with the nerve fascicles. Improvements in fabrication methods were implemented to target the polyLIFE's original mechanical weakness resulting in superior mechanical properties such as metal and insulation adhesion, fatigue, and tensile strength (Lawrence, Dhillon et al. 2004).

Intraneural Electrodes

Intraneural electrodes are the most invasive method of interfacing the PNS but offer the advantage of an increase in the signal-to-noise ratio and higher selectivity for signal acquisition and stimulation of the nerve. The most basic intraneural electrode designs involve the blunt penetration with needle-like electrodes through the perineurium with the ultimate goal of placing these electrodes in close proximity to peripheral axons for the excitation or action potential retrieval of such while also reducing the stimulation threshold by factors of 10 to 100 (Branner and Normann 2000). The Utah electrode array UEA consists of either 25 or 100 electrodes on a 2 x 2 mm or 4 x 4 mm base, respectively. Through the use of a pneumatic insertion device the UEA is inserted through the epineurium with minimal trauma to the nerve (Branner and Normann 2000). Enhancement to the basic design of UEA include the addition of different lengths (0.5-1.5 mm) of the needle-like electrodes in order to eliminate redundancy of axon targeting, thus creating the Utah slant electrode array (USEA) (Branner, Stein et al. 2001). The electrodes are placed in a row by column configuration and at each row the electrode increases (or decreases, depending on orientation) in height. The level of invasiveness of these electrodes requires the coating of biocompatible materials of such, which can also hinder the transduction of such devices. Thus, the USEA requires preparatory steps of the electrodes tips before implantation (Navarro, Krueger et al. 2005; Yoo, Sharma et al. 2012). The design of USEA has proven to be better than cuff electrodes in terms of current requirements to produce half-

maximum force in the target muscle (10.6% less) while having 4.3 times broader recruitment curve (Branner, Stein et al. 2001).

Regenerative electrodes achieve the same level of invasiveness and specificity as penetrative electrodes but in a different manner. This electrode type takes advantage of the regenerative properties of neurons restricted to the PNS, as opposed to those in the CNS (Fu and Gordon 1997; Horner and Gage 2000). Conceptually, the peripheral nerve is transected, followed by the implantation of a cylindrical structure (technically referred to as the nerve guidance conduit (NGC)) housing the electrodes through which the nerve is expected to regenerate across. The use of regenerative electrodes for PNS interfacing is greatly justified for amputee because the target nerve would not have a specific function, yet the nerve itself would remain functional (Kim and Romero-Ortega 2012). Regenerative electrodes are dependent on the level of regeneration of the transected peripheral nerve, which depends on the age and distance of the lesion from the cell body (Faweett and Keynes 1990). Additionally, a balance between the amount, size, or shape of the electrodes which would be mounted on the NGC must also be met in order to accomplish adequate nerve regeneration and the desired neural activity recording. For the past 40 years several techniques have been implemented for regenerative electrodes; from the material, to the structural design, to the addition of neurotrophins and proteins within the lumen of the NGC, to carbon nanotube coating of the electrodes (Navarro, Krueger et al. 2005; Keefer, Botterman et al. 2008; Lotfi and Romero-Ortega 2011). Advances in miniaturization t techniques allowed for the ratio of electrode to regenerating axon to be approximately one; however, this design places a restrictive effect on the regenerating axons due to the reduction of space through which the axons would be expected to regenerate through. Research indicates that the larger the transparency factor of a sieve electrode the more favorable results will be observed in terms of nerve regeneration (Zhao, Drott et al. 1997; Wallman, Zhang et al. 2001; Navarro, Krueger et al. 2005). Specificity of axon signal recording must be sacrificed in

order to obtain acceptable regeneration through the NGC. Materials for the NGC vary from polyurethane outer structure and a collagen-based gel in the lumen, to all-silicon, to polyacrylonitrile–Polyvinylchloride NGCs (Heath and Rutkowski 1998; Seifert, Desai et al. 2011; FitzGerald, Lago et al. 2012). Biocompatibility, ultimate tensile strength, and young modulus are key factors of NGCs. No immune response from the NGC while a sufficiently high ultimate tensile strength and a young modulus similar to that of the nervous tissue are desired (Yucel, Kose et al. 2010). Biocompatibility will prevent the electrode array implant from either host rejection or inadequate nerve regeneration (Heath and Rutkowski 1998). Silicon sieve electrodes with hole size of 30 μm and a transparency of 30% have demonstrated promising results for their use in neural prosthetics due to the degree of nerve regeneration achieved (Wallman, Zhang et al. 2001). Our lab has recently developed a regenerative multielectrode interface (REMI) that is placed between the distal and proximal of a transected rat sciatic nerve and is capable of acquiring single and multiaxonal signals as early as 7 days. The REMI consists of 18 needle-like platinum-iridium electrodes coated with parylene-C facing the lumen of a collagen-filled polyurethane NGC. High signal-to-nose ratios action potentials have been recorded using the REMI in some animals for as long as 120 days post implantation, which promises long term reliability for signal acquisition (Seifert, Desai et al. 2011; Kim and Romero-Ortega 2012). The invasiveness of regenerative and penetrative electrodes allow for single-axon action potential recording and selective stimulation. The required invasive surgery is justified for amputees for the potential increase in quality of life that these interfacing electrodes may provide through the use of neural prosthetics. Figure 1-5 summarizes the different approaches for interfacing the nervous system, of which the PNS offers more options. Figure 1-6 summarizes the different types of PNS interfacing electrode models.

Interfacing Electrode Enhancements

Electrode structure and design i.e., size, shape,, and cross-sectional area, have shown to be an insignificant factor in terms of foreign body response (Szarowski, Andersen et al. 2003). Szarowski et al. demonstrated that size, surface characteristics, insertion techniques, and even electrode-tip geometries resulted in similar foreign body response despite eliciting different wound healing response. Moreover, different materials have not shown a significant difference in immune response (Ignatius, Sawhney et al. 1998). Researchers are being challenged by the virtually-unavoidable foreign body response which is believed to be the primary factor leading interfacing failure over long periods of implantation (Polikov, Tresco et al. 2005). Despite foreign body response being practically proven as the primary cause of electrode interfacing failure in the CNS, the role of this mechanism has not been proven for the PNS; rather, recent research indicates that scar formation around the electrodes does not play a

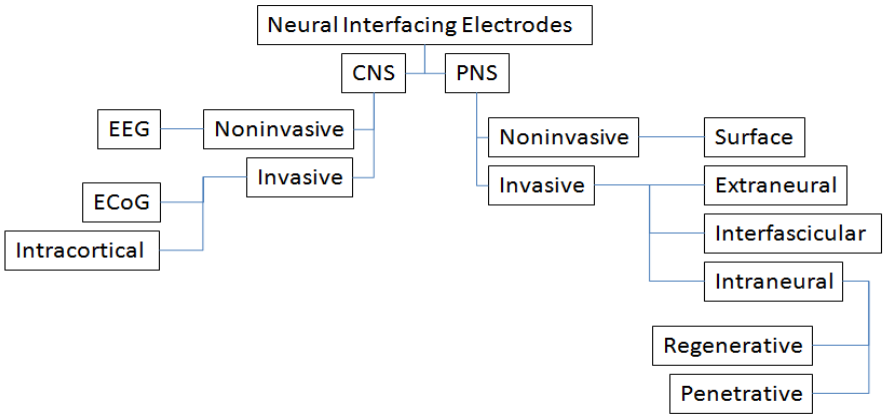

Figure 1-5 Neural interfacing methods. The first branch divides interfacing electrodes for the CNS and PNS. Interfacing the of the central nervous or peripheral nervous system can be achieved noninvasively or invasively

	PN Electrode	Materials	Schematic Diagram of PNI Electrode
Circum-neural	FINE	E: Pt, S: Silicone	
Interfascicular	polyLIFE	Kevlar fiber metalized with Ti, Au, and Pt, I: Silicone	
	LIFE	Pt-Ir wire, I: Teflon	
	TIME	E: Pt, S: Polyimide	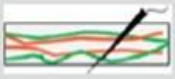
	CWIE	E: Nylon coated stainless steel	
Intraneuronal	USEA	E: Silicon with Pt tip, I: Silicon nitride, S: Silicon	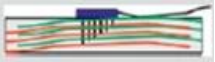
Regenerative	Sieve	E: Drilling holes into epoxy	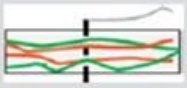
		E: Multiple-hole silicon	
		E: Flexible polyimide	
	REMI	E: Pt-Ir, I: Parylene-C	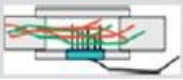
	MCRE	E: Au, S: Polyimide	
		E: Au, S: PDMS	

Figure 1-6 Summary of the PNS interfacing electrodes (adapted from(Kim and Romero-Ortega 2012))

major role in the signal decay (Khobragrade 2011). Alterations of the interfacing electrodes with various types of coatings and surface chemistry modifications are currently taking previous electrodes models to the next level. Lower charge injection capacity metals are becoming more widely used because of their efficacy and safety when eliciting a desired physiological response—whether it is initiating or suppressing an action potential (Merrill, Bikson et al. 2005). Chemically modifying surfaces with carbon nanotubes (CNTS) has also proven to enhance the safety, function, and longevity of extracellular electrodes. CNTS fabricated via the layer-by-layer (LBL) method are capable of withstanding the long-term stresses and physical conditions found within the human body (Mamedov, Kotov et al. 2002; Green, Lovell et al. 2008;

Jan, Hendricks et al. 2009). Laminin (a glycoprotein of the extracellular matrix) coatings of a few nanometers in thickness fabricated by LBL assembly have been proven to produce minimal impact on the structure of electrodes or their low impedance values while encouraging neural growth and lessening immunoreactivity (gliosis) (Ignatius, Sawhney et al. 1998; He and Bellamkonda 2005; He, McConnell et al. 2006; Bossi, Benvenuto et al. 2010). Collagen, the most abundant protein in humans, has shown promising results as an electrode performance enhancer for its ability to provide topographical cues that allows the outgrowth of neural tissues on electrodes (Di Lullo, Sweeney et al. 2002; Liu, Houle et al. 2012; Zarbin, Montemagno et al. 2012). Gold electrodes treated with polypyrrole (PPy) and poly(3,4-ethylenedioxythiophene) (PEDOT) coatings are enhanced by decreasing their impedance and thus increasing their charge transfer by two or three order of magnitude, which allow researchers to obtain higher signal-to-noise recordings (Jan, Hendricks et al. 2009; Venkatraman, Elkabany et al. 2009). Because the proximity of neurons correlates directly with signal strength, strategies which encourages the growth of neurons near the electrodes are being devised (Polikov, Tresco et al. 2005). Adhesion molecules and nerve growth factors are also currently being studied as potential enhancers of nerve interfacing electrodes (Kim and Romero-Ortega 2012). Nerve growth factor (NGF) suspended in hydrogels have been used to improve the neural signal readings from iridium-oxide electrodes through the slow release of NGF, which has the capacity to rescue apoptotic dorsal root ganglion subsequent to nerve crush and sciatic nerve transaction (Donnerer 2003; Winter, Cogan et al. 2007). Although NGF and brain-derived neurotrophic factor (BDNF) have been found to stimulate the regeneration of axons from adult DRG neurons *in vitro,* much research is still necessary to fully observe and characterize the potential of neurotrophins as electrode coatings or components (Lindsay 1988; Kim and Romero-Ortega 2012). Experiments also point to the potential of incorporating or culturing adhesive cells on the interfacing devices to increase the integration in the host

with the advantage that these cells are not likely to cause impedance changes in the electrodes (Merrill and Tresco 2005).

Interfacing Electrode Limitations

Signal acquisition failure has been theorized to be a result to neural death or regression caused by implantation of electrodes (Edell, Toi et al. 1992; Turner, Dowell et al. 2000). Gradual signal strength decay indicates that there is a progressive microenvironmental change post-electrode implantation (Polikov, Tresco et al. 2005). Several mechanisms have been suggested to be responsible factors: increased electrical impedance as a diffusional barrier (Porter, Adey et al. 1964; Liu, McCreery et al. 1999; Weiland and Anderson 2000), increased distance between electrode and action potential source (Salcman and Bak 1976; Polikov, Tresco et al. 2005) (placement of the electrode within 130 µm of an action potential source will, in theory, be observed below noise; while experimental data indicates that the electrodes should be no farther than 50/100 µm (Eaton and Henriquez 2005; Polikov, Tresco et al. 2005)), mechanical failures (breakage of electrodes and/or associated wiring) (Carter and Houk 1993), and neural plasticity (Darian-Smith and Gilbert 1994; Navarro, Vivó et al. 2007). Previous research in our laboratory indicates that the percentage of active channels reaches a maximum of 60 percent after 21 days post REMI implantation. After reaching a maximum number of recording channels, the channels being to gradually fail, suggesting a progressive change within the nerve. By day 56 the number of active channels is approximately 10 percent. This trend is summarized in figures 1-7. Even if long-term implantation without electrode failure is possible, long-term amputees may face diminished control of a prosthetic due to neural pathway degeneration or atrophy, which may include central connections (Carlson, Lais et al. 1979; Hoffer, Stein et al. 1979; Dhillon, Lawrence et al. 2004). Permanent axotomy by amputation has been shown to result in loss of motor neurons in human with early contact with the distal

stump and/or target musculature being a significant factor for the survival of motor neurons (Kawamura and Dyck 1981; Tornqvist and Aldskogius 1994). Peripheral nerves that were transected and resutured to their respective distal stump or retargeted to a muscle showed recovery. These transected nerves, despite of having lower action potential amplitude values, were often able to achieve nerve conduction, muscle potentials, and twitch tension comparable to control values (Davis, Gordon et al. 1978). Thus, action at the clinical level must be taken in order to aid the survival of the proximal stump in order prevent axon atrophy and increase the potential of future amputees and neural prosthetic interfacing.

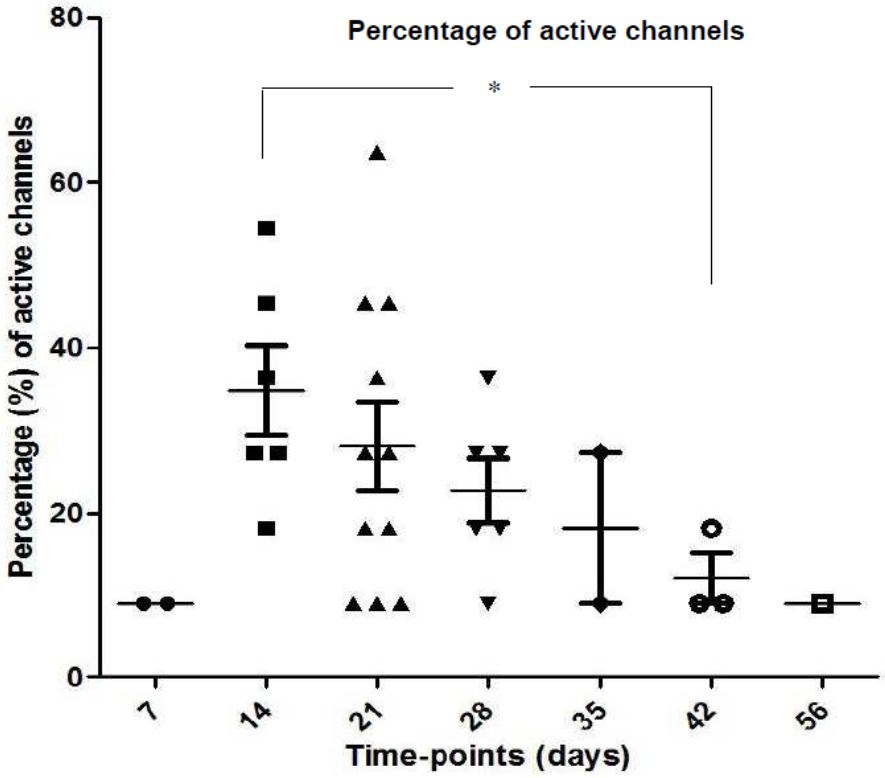

Figure 1-7 Decline in the percentage of active electrodes per implanted array after reaching a maximum percentage at 21 days. Asterisks (*) denote a significant difference at $p < 0.05$ with a one-way ANOVA test (Khobragade 2011)

Foreign Body Response

Foreign body response is initiated by the implantation of interfacing devices due trauma associated with probe insertion, materials, chemical coatings, geometrical and topographical characteristics of the electrode (Coleman, King et al. 2004; Biran, Martin et al. 2005). Host reactions post-implantation of interfacing electrodes include injury, blood-material reactions, provisional matrix formation, acute inflammation, chronic inflammation, granulation tissue development, foreign body reaction, and fibrous capsule development. The presence of mitogens, chemoattractants, cytokines, growth factors, and other bioactive components within the extracellular matrix of the affected area provide a rich milieu of activating and inhibiting substances capable of modulating macrophage activity as well as the proliferation and activation of other cell populations in the inflammatory and wound healing responses. The extent or degree of these responses is modulated according to the extent of injury in the implantation procedure, the tissue or organ into which the device is implanted, and the temporary formation of the matrix elicited by the implant. The acute response to an implantation is characterized by the polymorphonuclear leukocytes (PMNs). Mast cells degranulation, interleukin-13, interleukin-4 with histamine release and fibrinogen adsorption will also mediate acute inflammatory responses to implants, which usually lasts no more than a week. The presence of mononuclear cells (monocytes, plasma cells and lymphocytes) and macrophages mark the beginning of the chronic inflammation phase. The utilization of biocompatible materials will usually lead to the early resolution of the acute and chronic inflammatory responses within two weeks. Macrophage recruitment to the site of implantation is guided by chemokines (cytokines with chemo attractive properties) and other chemoattractants such as transforming growth factor (TFG-β), platelet, platelet-derived growth factor (PDGF), platelet factor 4 (PF4), interleukin (IL-1), and leukotriene (LTB4). Macrophages are activated and recruited in an attempt to phagocytose the implant. In a positive-type feedback loop, the same recruitment of macrophages to the

implant surface leads to further propagation of chemoattractive signals such as PDGF, tumor necrosis factor (TNF-α), interleukin-6, granulocyte-colony stimulating factor (G-CSF), and granulocyte macrophage colony stimulating factor (GM-CSF). After macrophage recruitment to the implant, macrophages undergo cytoskeleton remodeling in order to spread over the material surface. Once activated and recruited to the site of implantation, macrophage secretions of growth and angiogenic factors are capable of regulating fibro-proliferation and angiogenesis. Furthermore, activated macrophages over express extra cellular matrix (ECM) proteins such as fibronectin and are involved in the remodeling of the injured tissue .The disruption of adhesion to the surface of the implant leads to anoikis, a term of apoptosis. Thus, material surface chemistry can influence a prolonged chronic inflammation by influencing attachment to the surface of such, or reduce the inflammation response by promoting detachment of macrophages and eventual apoptosis (Anderson, Rodriguez et al. 2008). Figure 1-8 illustrates the well-known foreign body response to electrodes implantation in the central nervous system, which has similar initial response, but with final difference in cell-type recruitment i.e., microglia and astrocytes (Schwartz, Cui et al. 2006).

The injury and trauma to the peripheral nerve elicited by the implantation of the REMI has been previously studied under acute amputation conditions (Khobragade 2011). Khobragade concluded that the chronic inflammation, measured by the number of macrophages and fibroblasts within the scar region around the explanted electrode shaft, gradually decreased through the 15, 30, and 60 day time periods tested. Moreover, the scar density (defined as the scar area divided by the number of macrophages and fibroblasts), remained constant. It has been documented that the foreign body reaction at the tissue/material interface is present for the *in vivo* lifetime of the implant(Anderson, Rodriguez et al. 2008), which explains the persistence of the macrophage recruitment to the electrodes of the REMI—even after 60 days of implantation. The foreign body response to REMI implantation after subchronic

amputation, however, has not been evaluated. Thus, this thesis partly focuses on the study of the chronic inflammation caused by the implantation of the REMI post subchronic amputation. Based on previous reports about biocompatible implants, It is expected that neither the acute or chronic inflammatory response elicited from the initial injury (amputation simulation surgery) will have an effect on the REMI implantation because these two events resolve in approximately two weeks (Anderson, Rodriguez et al. 2008), whereas the REMI implantation takes place four weeks after the initial injury. Therefore, the inflammatory responses from these two separate injuries are not expected to overlap. However, It has also been numerously suggested that after injury to the peripheral nerve and subsequent Wallerian degeneration, macrophages will permeate and remain at the affected site over at least one month period while they remove the majority of the myelin debris (Fenrich and Gordon 2003). Ergo, more studies are needed to fully evaluate the foreign body response to REMI implantation after subchronic amputation.

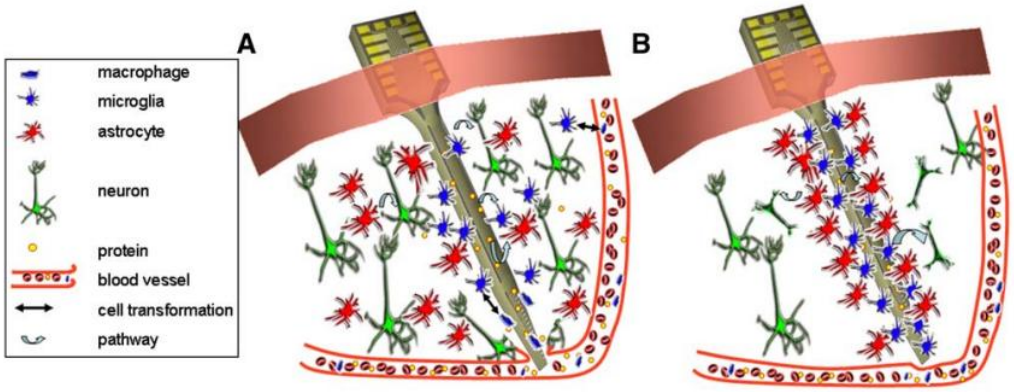

Figure 1-8. Foreign body response to electrode implantation in the CNS; (A) acute response, (B) chronic response (Schwartz, Cui et al. 2006)

Peripheral Nerve Regeneration

Peripheral nerve injury initiates the rapid influx of signals that contribute to cellular stress which induces transcription factors, adhesion molecules, growth-associated proteins, and structural components needed for peripheral axonal elongation (Seifert, Desai et al. 2011). Axotomy causes the distal and proximal nerve stumps to retract, axoplasm leaks out and the membranes (epineurium, perineurium, endoneurium) collapse. Axons physically separated from the cell body degenerate, followed by the infiltration of leukocytes to the affected area, the formation of ovoids as Schwann cells fragment the myelin sheaths, and the transformation of Schwann cells from myelinating to nonmyelinating, a process otherwise known as Wallerian degeneration (Fenrich and Gordon 2003). Macrophages, recruited through cytokines, enhance the lysis and phagocytosis of the myelin and subsequent Schwann cell proliferation. Neurotrophic factors produced by Schwann cells in the distal stump enhance the nerve regeneration after injury. A second phase of Schwann cell proliferation, mediated by neurotrophic factors specific for glial cells, occurs when Schwann cells come into contact with the regenerating axons. If axonal regeneration is delayed, Schwann cell number decreases progressively and become less sensitive to axonal regeneration (Terenghi 2002). Neurons and the Schwann cells of the PNS progressively fail to sustain the regenerative response with time after injury (Fenrich and Gordon 2003). While Wallerian degeneration takes place in the distal stump of the peripheral nerve, the proximal nerve stump undergoes a “die back” process, where the axon reverts back to the nearest node of Ranvier. If the injured axon is located within a growth permissive environment, e.g., presence of growth-supportive nonmyelinating Schwann cells and no chronic injury, the upregulation of RAG genes will lead to the formation of growth cone stability and elongation as well as axonal guidance and sprouting. Also, the upregulation of tubulin and actin coupled with reduced neurofilament-tubulin ratio which in turn reduces neurofilament interactions, allows

axons to regenerate at 1-3 mm/day. The molecular signals that drive the transformation of nonmyelinating Schwann cells toward myelinating Schwann cells are mainly derived from adherence to an axon destined for myelination and the basal lamina (Jessen and Mirsky, 1999). ECM molecules of the basal lamina and their receptors have an active role in axonal elongation and in remyelination via interactions with glial cells. Upregulation of laminin, fibronectin, and specific integrins, which are present during embryo development, contribute to the remyelination process (Akassoglou, Yu et al. 2002). Previous studies peripheral axonal regeneration and remyelination after REMI implantation under acute amputation conditions revealed the inability of the axons to be completely remyelinated after 15 days (Seifert, Desai et al. 2011). Furthermore, it has been well documented that complete remyelination of the peripheral nerve after being completely demyelinated via lysophosphatidyl (LPC) injections takes approximately 20 days (Smith and Hall 1980). The present study aims at correlating the axonal growth and remyelination with the foreign body response to REMI implantation under subchronic implantation in order to evaluate the effect such events and to elucidate the eventual interfacing failure of the REMI.

Blood Nerve Barrier

The blood nerve barrier (BNB) is a functional barrier between the peripheral nervous system and the circulatory system (Poduslo, Curran et al. 1994). The BNB is composed of endoneurial microvasculature and other inner layers of the perineurium. Vessels are located along the length of the peripheral nerves; these vessels branch numerously on the nerve surface to form a complex anastomotic plexus on the epineurium. Small vessels penetrate into the intrafasciular space to form an endoneurial vascular network that is composed of mainly capillaries running along the length of the nerve. Blood vessels in the endoneurium are lined by a continuous endothelium with intercellular tight junctions (TJs). Together with the perineurium, the vessels form a

blood-nerve barrier to regulate the microenvironment in the endoneurium of nerve. TJs between adjacent peripheral nerve microvascular endothelial cells (PnMECs) are responsible for BNB function (Kashiwamura, Sano et al. 2011). Studies have proven that these tight junctions are known to prevent the influx into the endoneurium of particles with a radius of 1.15 Å and a molecular weight of 139 Daltons. However, hypertension created in endoneurial vessels is capable of damaging the BNB, rendering it leaky and allowing the unregulated diffusion across the endoneurium. Overall, the impermeability properties of the BNB are due TJs, which adjoin adjacent capillary of the perineurial sheath, which ultimately restrict intercellular diffusion across the cell layers as a whole (Rechthand and Rapoport 1987). Myelinating Schwann cells are responsible for the formation autotypic junctions in the Schmidt Lanternman incisures, paranodal loops, mesaxons and the outer aspect of the nodal gap. This indicates that while the peripheral nerve is regenerating following the implantation of a REMI, there will not be an abundance of tight junctions due to the initial lack of remyelinating Schwann cells. More specifically, as the axons regenerate through the lumen of the REMI and past the electrodes, there will not be a significant amount of TJs among the Pt/Ir electrodes of the REMI. However, as the peripheral axons regenerate and the Schwann cells transform from nonmyelinating to myelinating phenotype, the TJs form and organize. Autotypic tight junctions have been numerously proposed to function as a permeability barrier, separating the extracellular space outside the myelin sheath from the intramyelinic space between the lamellae. (Poliak, Matlis et al. 2002). This study suggests a new direction in the research for interfacing electrodes. It is hypothesized that as the nerve regenerates, the perineurial cells will organize around the electrodes and foreign body response cells, forming the perineurium and hence the BNB, which will limit the ion influx of action potential depolarization ions to come in proximity with the electrode tip and hence hinder the signal acquisition of the electrodes.

Clinical Relevance of Present Study

Following an amputation procedure, the subject is expected to practice with the artificial limb no earlier than 10 to 14 days after the surgery, depending on the comfort and wound healing process (John Hopkins Medicine). However, this type of recuperation takes place under ideal circumstances; in most cases it would take 6-8 weeks before patients are stabilized and eligible for neural interfacing. Thus, newly amputees would not be interfaced acutely following the amputation procedure. Furthermore, due to the lack peripheral nerve interfacing electrodes available at the clinical level, practically all amputees today are considered and will be considered non-acute amputees. That is, most amputees are either categorized as chronic or subchronic amputees. Thus, testing and evaluating the REMI post subchronic amputation has direct implications to the potential clinical studies of interfacing electrodes for the control and feedback sensation of robotic prosthetics.

Specific Aims of the Project

Our laboratory recently developed and tested a regenerative multi-electrode interface (REMI) with an open architecture for the nerve to regenerate and come in contact with 18 electrodes under acute amputation conditions. It is hypothesized here that 1) REMI implantation under subchronic amputation conditions yields comparable results to acute amputation model in terms of foreign body response and nerve regeneration and 2) the BNB formation is directly involved in the progressive failure of interfacing electrodes. The study presented here aims at testing the REMI under subchronic amputation conditions to evaluate foreign body response, nerve remyelination and BNB formation via immunohistochemistry to test these hypotheses.

SPECIFIC AIM 1: To evaluate the foreign body response to REMI interfacing after a sub chronic nerve injury.

SPECIFIC AIM 2: To determine the quality of peripheral nerve regeneration in 30-day amputation injuries.

SPECIFIC AIM 3: To assess the extent blood nerve repair after REMI neural interfacing.

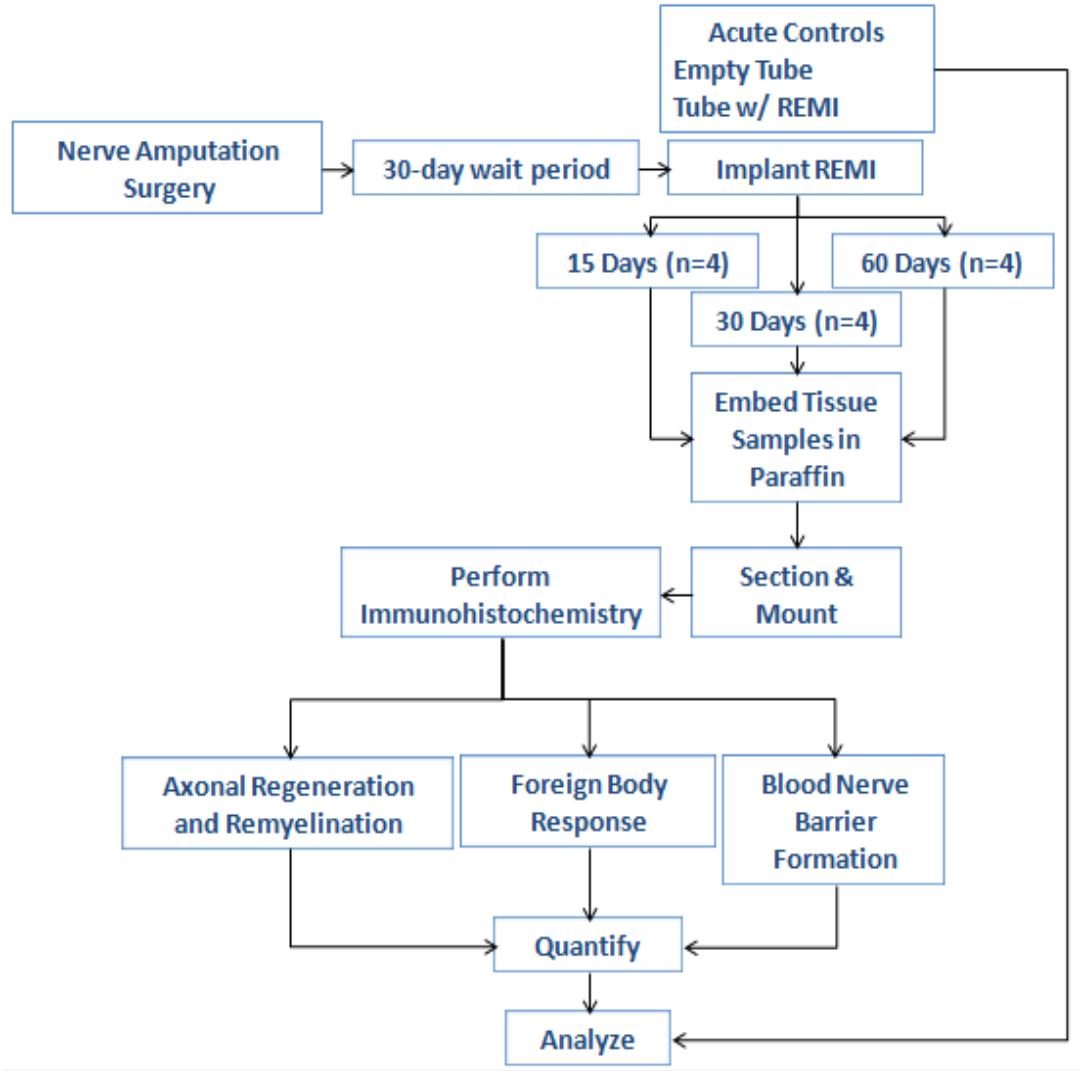

Figure 1-9. General overview of thesis experimental procedure

Chapter 2

Foreign Body Response

Background

Foreign body response to implants directly affect the performance to implanted medical devices (Coleman, King et al. 2004; Polikov, Tresco et al. 2005). Electrode implantation failure in the CNS has been well-theorized (Merrill and Tresco 2005); thus this study aims at elucidating the foreign body response to implanted REMIs post 30-day subchronic amputation in the sciatic nerve of rats at 15, 30, and 60 day time post-interfacing. The nerve tissue samples were labeled for ED1 reactive macrophages at each time point with the intent to identify a pattern in the scar formation. The density and size of the scar was also correlated with the nerve regeneration and formation of the blood-nerve barrier, which will be discussed more in depth in Chapter 3 and 4.

ED1 antibody has been well-established as a marker for free or fixed cytoplasmic antigens in monocytes as well as most macrophages (Dijkstra, Döpp et al. 1985). Macrophage invasion (labeled with ED1 antibody) of biocompatible NGC have been previously shown to be moderate; moreover, previous results from our laboratory have shown an immune response to the REMI implantation after acute amputation (Keilhoff, Stang et al. 2003; Seifert, Desai et al. 2011). A recent study has dispatched micromotion as a possible factor for chronic immune response to the implantation of REMIs through the study of Activating Transcription Factor 3 (ATF3). However, scientists still speculate that mechanical shear forces created by the NGC on the surroundings soft tissues is a plausible factor of continued immune response (Rosengren, Danielsen et al. 1999; Huebsch and Mooney 2009). Due to the lack of knowledge on the immune response to peripheral nerve implant after a subchronic amputation, this chapter focuses on the host response to an implanted REMI.

Methods

Chronic Amputation

A total of 12 Lewis rats (215 -275 g) were used for immunohistological purposes. The animals were anesthetized with isoflurane (5% induction, 2%-2.5% maintenance) in 100% oxygen. When the animals had lost corneal reflex, their dorsal surface was shaved and cleaned with povidone-iodine. The sciatic never was exposed through a muscle-sparring incision along the sciatic vein between the semitendinosus and the biceps muscles. The two muscles were gently spread to expose the sciatic nerve. At this point the nerve was transected, giving rise to the distal and the proximal nerve stumps. The distal nerve stump was ligated with silk thread and the proximal nerve stump was sutured to the biceps femoris as pictured in figure 2-2 A. The skin was closed using staples and all the animals were administered with antibiotic (cephazolin; 5 mg/kg, IM) and analgesic (buprenorphine 0.05 -0.1 mg/kg SC) treatment post-surgery. All procedures were performed in accordance with the guidelines of the Institutional Animal Care and Use Committee (IACUC) of the University of Texas at Arlington (UTA).

REMI Fabrication

Custom-made floating array with 18-pin Parylene-C insulated Pl/Ir electrodes were used (150-300 kΩ impedance, Micropobes Inc., Gaithersburg, MD). Each electrode was approximately 50 µm at the shank, varied in height from 0.7 to 1.0 mm, and were place 400 µm apart to maximize contact and avoid redundancy with the regenerating nerve fibers. The array cable was fabricated from Parylene-C insulated 25-µm gold wires wound in a helixand coated with Nusil-type MED6-6606 nonrestrictive silicone elastomer and was 4.5 cm in length. The cable was bound to an Omnetics connector (Minneapolis, MN), housed in a titanium pedestal. Approximately 0.7 mm long polyurethane (Micro-Renathane, Braintree Scientific, Inc., Braintree, MA) tubes were

cut, and then a 2 mm by 2 mm square was cut on top of the tube to allow the housing of the electrode array. Prior to implantation, the tubes were sterilized and filled with collagen-I/III (0.3% Chemicon, Temecula, CA). Figure 2-1 illustrates the REMI design.

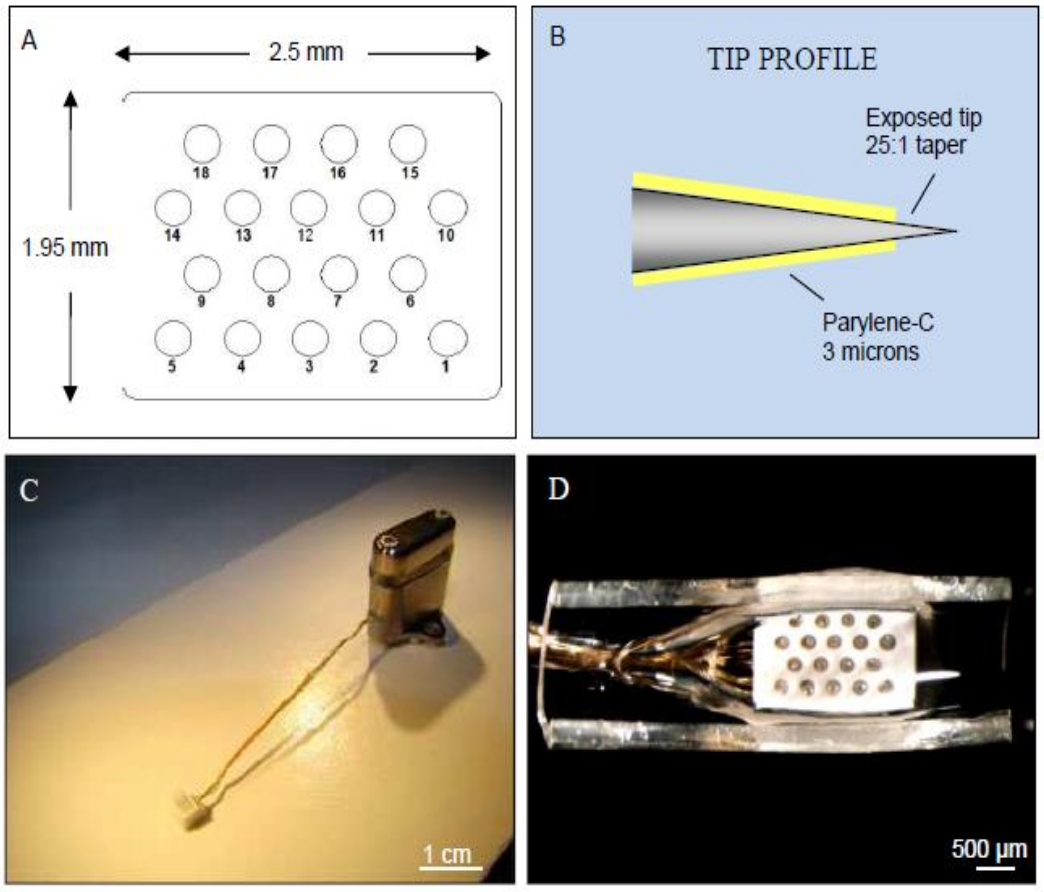

Figure 2-1 Structure of Regenerative Multi-electrode Interface (REMI). A) Configuration and dimensions of the floating multi-electrode array. B) Profile of the electrodes coated with parylene-c; the tips are exposed for signal acquisition purposes. C) Titanium pedestal encasing an Omnetics connector linkin the microelectrodes via parylene-c coated gold wires. D) REMI inlaid in the polyurethane NGC

REMI Implantation

Thirty days after the initial transaction of the sciatic nerve, the animals were anesthetized with isoflurane (5% induction, 2%-2.5% maintenance) in 100% oxygen. When the animals had lost corneal reflex, their dorsal surface was shaved and cleaned with povidone-iodine. The sciatic never was exposed through a muscle-sparring incision along the sciatic vein between the semitendinosus and the biceps muscles. The two muscles were gently spread to expose the previously transected sciatic nerve. The original proximal nerve stump which had been transected and sutured to the biceps femoris was retransected. The new proximal and distal nerve stumps were introduced into opposite ends of a sterile tube or REMI and sutured in place as shown in figure 2.1 B. The REMI is connected to an 18-pin connector housed in a silicone-sealed titanium pedestal, which was mounted on the pelvis with bone cement (Biomet; Warsaw, IN). The skin around the pedestal was closed using staples and the animals were provided with antibiotic (cephazolin; 5 mg/kg, IM) and analgesic (buprenorphine; 0.05-0.1 mg/kg, SC) post-surgery. All procedures were performed in accordance with the guidelines of the IACUC of UTA.

Sciatic Nerve Harvesting and Sample Preparation

Twelve REMI-implanted animals were sacrificed 15 day, 30 days, and 60 days post REMI implantation (preceded by a 30-day period of chronic amputation simulation). The animals were euthanized with an intraperitoneal sodium pentobarbital (100 mg/kg) injection. Transcardial perfusion was then performed on the animals with 0.9% saline for 5 minutes, followed by 4% paraformaldehyde (PFA) for 15 min. The regenerated nerve and REMI are harvested and post-fixed overnight in 4% PFA and then transferred to 1X

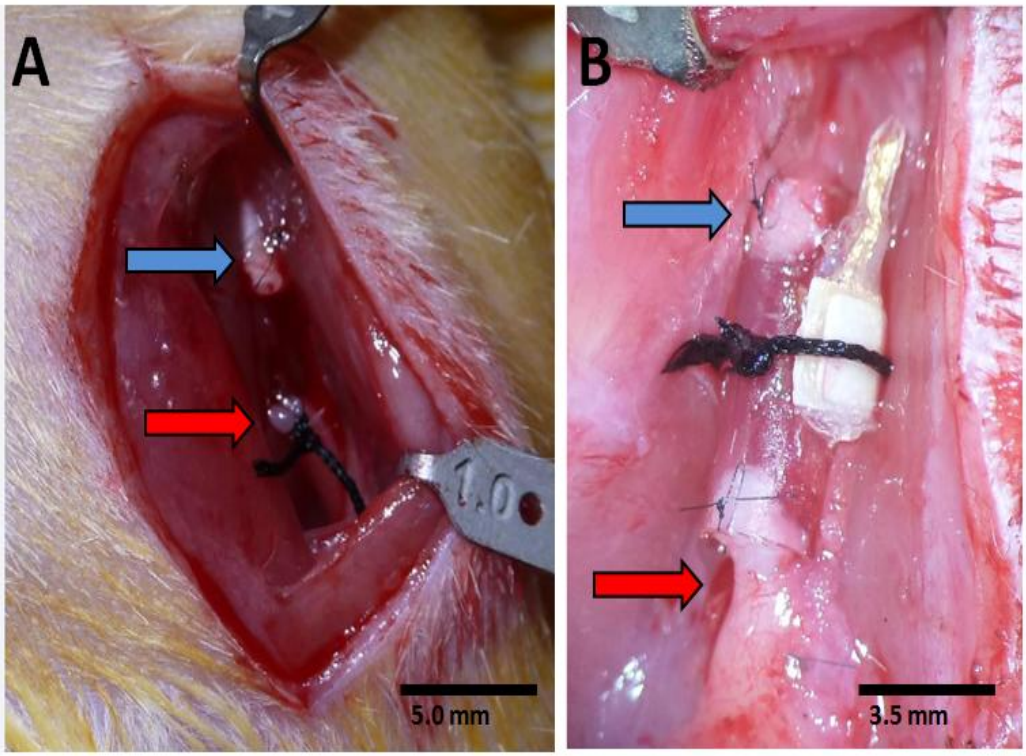

Figure 2-2 Nerve amputation (A) and REMI implantation surgery (B). A) The distal nerve stump (red arrow) is ligated with silk thread and the proximal nerve stump (green arrow) is sutured to the biceps femoris. B) REMI implantation after 30 days of chronic amputation. The originally proximal nerve stump end (figure 2.1 A) developed a neuroma (red arrow) and became the new distal nerve stump, while the proximal nerve stump (blue arrow) remains unchanged

phosphate buffered solution (PBS). The polyurathane tube was then removed as shown in figure 2-3 and the tissue was marked for its proximal (green dye) end, distal (red dye) end, and orientation of electrode (blue dye). The nerve tissue sample was then embedded in paraffin wax for histological studies. The paraffin-embedded nerve sample was sectioned at 6 µm – 10 µm thickness and mounted on positive-charged slides.

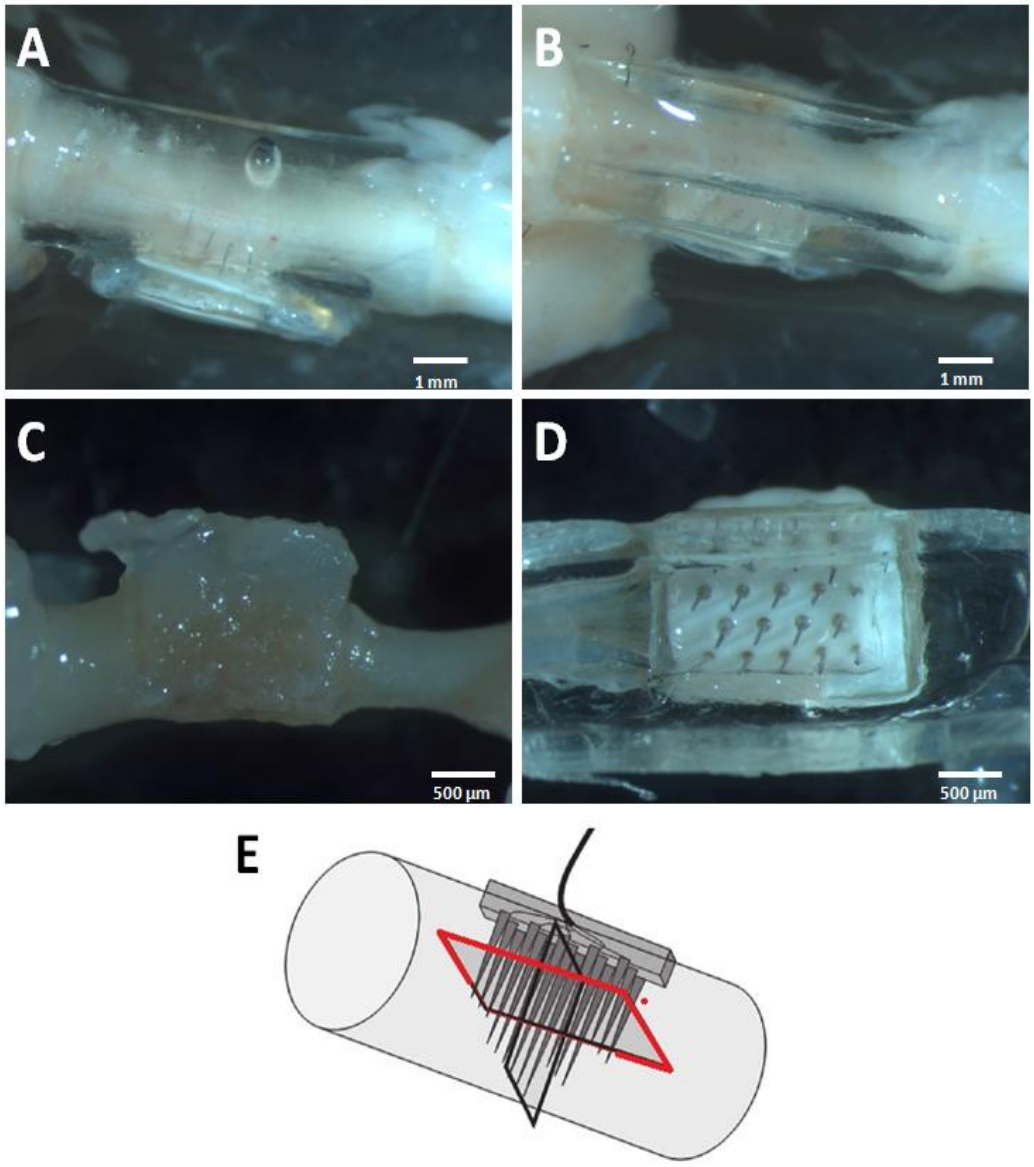

Figure 2-3 REMI structure with and without regenerated nerve. REMI shown after extraction and riddance of fibrotic and muscle tissue residue (A) and opened structure of the REMI with the sciatic nerve still inside (B); nerve sample (C) removed from REMI (D) and schematic of the REMI with the horizontal plane of sectioning and immunelabeling shown in red (E) (adapted from (Garde, Keefer et al. 2009)

Immunofluorescence Staining

The sectioned (plane shown in figure 2-3 E) and mounted nerve tissue samples were placed in an oven at 58-60˚ Celsius for 30 minutes to facilitate the attachment of tissue and to soften the paraffin. The tissues were then rehydrated in by placing them in two baths of xylem for five minutes each, followed by two baths of 100% EtOH for three minutes each, then one bath of 90% EtOH for three minutes, then one bath of 70% EtOH for 3 minutes, and finally a bath in DI water for 10 seconds. Epitope retrieval was accomplished with a citric acid bath at 80-85˚ Celsius for 15 minutes. Then the citric acid bath was allowed to continue for another 20 minutes at room temperature. A three-minute DI water bath was performed and then two baths with 1X PBS for 5 minutes on orbital shaker. The slides were dried and hydrophobically marked to prevent the primary and secondary solutions to escape the slide. 500 µL of blocking solution (4% normal goat serum (NGS), 0.5% Triton X in 1X PBS) was added to each slide for one hour. Then three baths of washing solution (1X PBS and 0.5% Triton X) for 15 minutes each were performed. Finally, the primary antibodies were added (mouse anti-ED1, Millipore, 1:250 dilution rate). Twelve hours later, the samples were washed three times with washing solution for 15 minutes each, and once with 1X PBS for 15 minutes. The secondary staining (IgG Dylight 488, 1:400 dilution rate) in washing solution was then performed and incubated for one hour. The samples were washed three times with washing solution for 15 minutes each, and once with 1X PBS for 15 minutes. The slides were then mounted for Confocal/fluorescent microscope studies.

Imaging and Quantification

Pictures were taken of the sciatic nerve post-immunohistochemistry steps using a confocal microscope (Zeiss LSM 510) with three single photon lasers (Ar, HeNe 543, HeNe 633) which allow the user to select lines of 458, 488, 514, 543, 568, and 633 nm. For our purposes, the filters were set up to allow lines of 488 and 633 to visualize the

anti-mouse DyLight 488 secondary antibody (mouse anti-ED1 primary) and TO-PRO-III (nucleic counter stain), respectively.

The area of the macrophage scar around the explanted electrode site and the macrophage cell density were quantified using ImageJ software. The scar area was identified by the ED1-positive cells and the area encompassing these cells was measured (excluding the area of explanted electrode). The amount of cells within the scar was identified by the number of T0-PRO-III- positive signals. This process was performed on four electrode perforations per animal. The average of all the values was obtained using the AVG function in MS EXCEL. Figure 2-4 portraits the quantification process; figure 2-5 illustrates the methodology for scar area quantification.

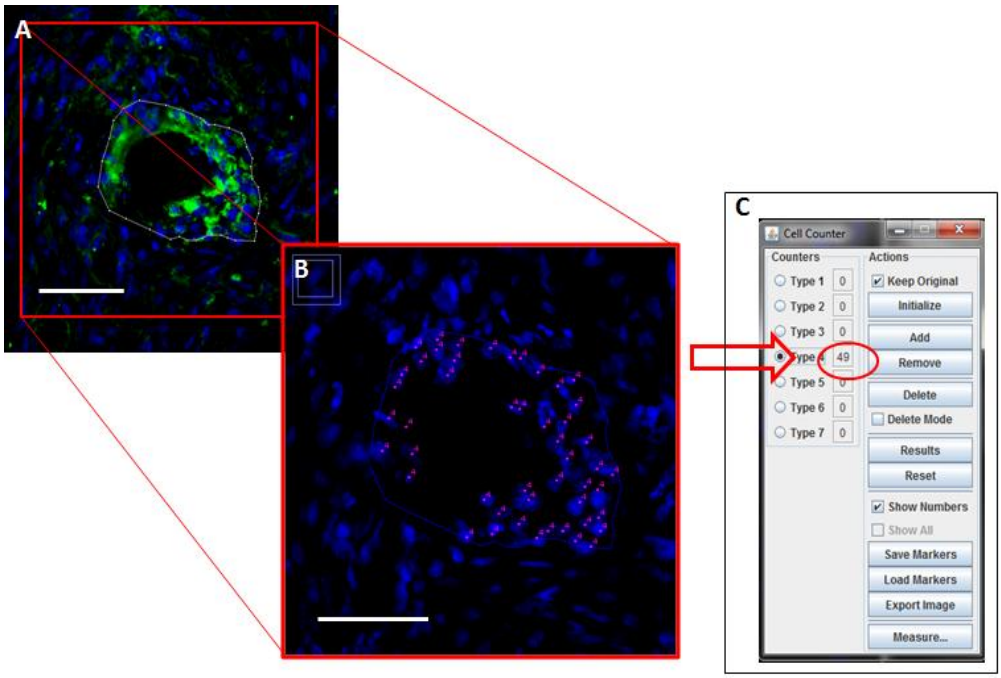

Figure 2-4 Quantification of cell population within scar region (A) via immunolabeling of ED1 and TO-PRO-3 (B) and quantified with ImageJ software (C). A) Shows the ED1 staining and TO-PRO-3 staining merged images with a white line denoting the scar region. B) Shows a zoomed-in image of the scar region (marked with blue line) and the TO-PRO-3 staining only to allow for quantification. Type 4 (magenta-colored dots)

counter was selected for its contrasting color against the TO-PRO-3 labeling. C) Shows the cell counter and the results for the specific image. Scale bar; 170 µm for all the images.

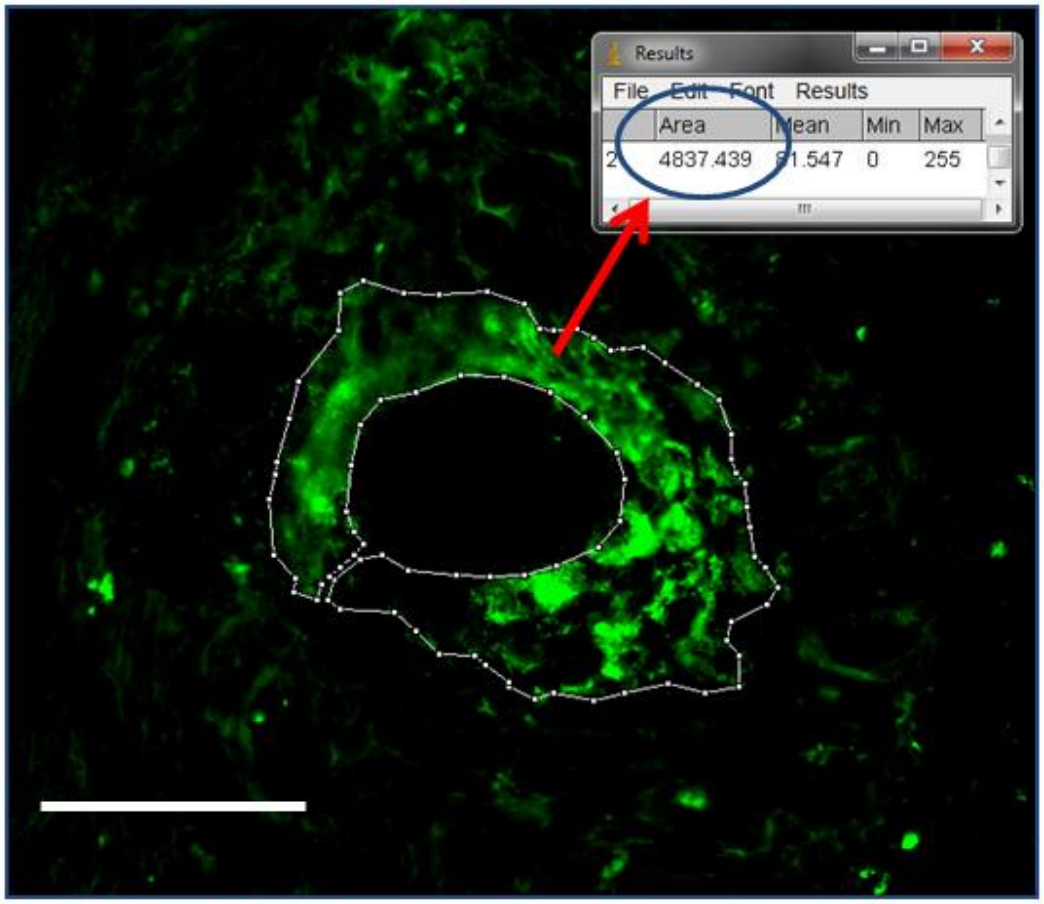

Figure 2-5 Quantification method for the scar area. The image shows ED1 labeling of macrophages with the successive scar region marked with a white line. The area was measured using the measuring tool in ImageJ. Scale bar; 70 µm

Statistical analysis

The area and cell density under acute amputation for 15, 30, and 60 days post-implantation were compared using one-way ANOVA followed by Neuman-Keuls comparison *post hoc* evaluation (Prism 6, Graphpad). P-values less than 0.05 were

considered statistically significant. The results were reported as mean ± standard error of the mean.

Results

The subchronically amputated samples showed diminished amount of nerve regeneration despite signs of robust tissue regeneration when compared to the acutely amputated nerve samples. The nerve bridge of the subchronically amputated samples showed an obvious size disparity in terms of girth when compared to the proximal side. The tissue regrowth on the REMI and within the REMI is shown in figure 2-3 A and figure 2-3 B, respectively. The polyurethane NGC was enveloped by vascularized fibrous and smooth muscle tissue in all the REMIs explanted, as demonstrated in figure 2-5 A. Furthermore, the number of electrodes perforations that could be observed within the subchronically amputated nerve tissue samples was 4 (n =12) compared to the 11 electrode (n=30 Lewis rats) perforations for the acutely amputated animals.

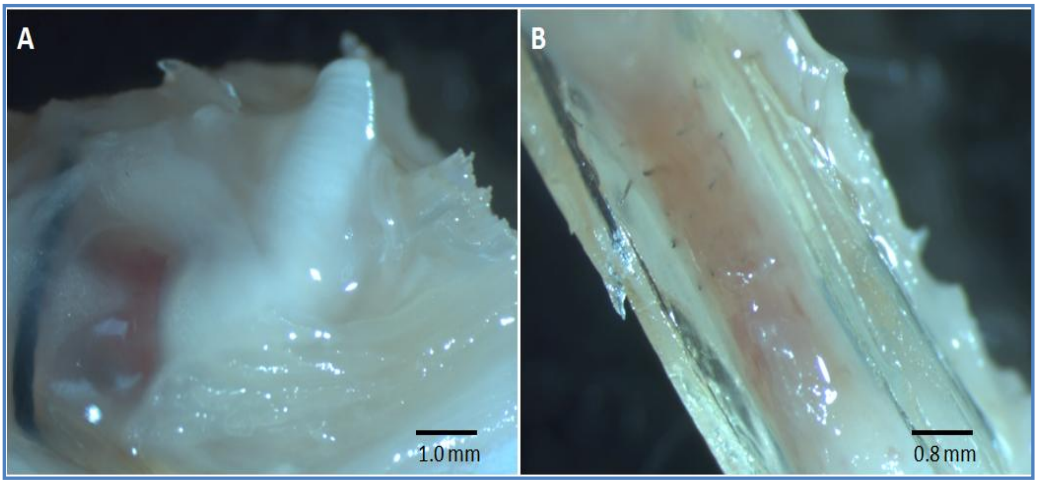

Figure 2-6 Tissue regeneration around (A) and within (B) the REMI. A). shows fibrotic and smooth muscle tissue regeneration on the REMI with the part of the nerve protruding (picture taken post-REMI explantation, 30 day time point). B) Shows l nerve tissue regeneration within the lumen for the subchronically amputated animals

The nerve samples were extracted from the NGC, as shown in figure 2-3 and immunohistochemistry was performed to mark the macrophages (ED1+ signal) and all nucleated cells (TO-PRO-3+ signal) present in the peripheral nerve tissue sample. The scar is also composed of fibroblast, which are nucleated cells and thus able to be marked with TO-PRO-III (Garde et al. 2009). Figure 2-7 qualitatively compares the progressive decrease in macrophage scar area through three time periods. Acutely and subchronically interfaced animals show an obvious decrease in the size of the

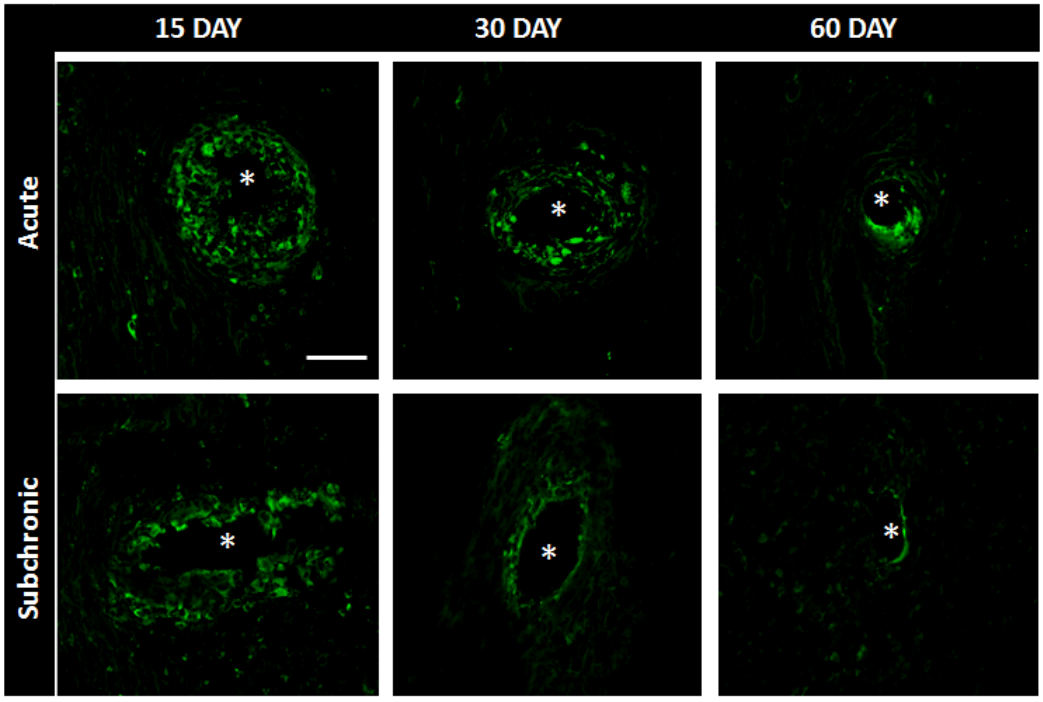

Figure 2-7 Progression of foreign body response immunolabled with ED1. Macrophages present at explanted electrode region: representative fluorescence images of ED1 positive labled cells at 15 day, 30 day, and 60 day time points for the acutely implanted REMI and the subchronically implanted REMI. Scale bar; 80 µm for all images. Asterisk (*) denotes electrode location within the tissue

macrophage between the 15 and 60 days post-REMI implantation. Cell density for the two groups show that the scar around the electrodes did not compact—however, a

quantitative approach was taken to better assess the progression of the foreign body response.

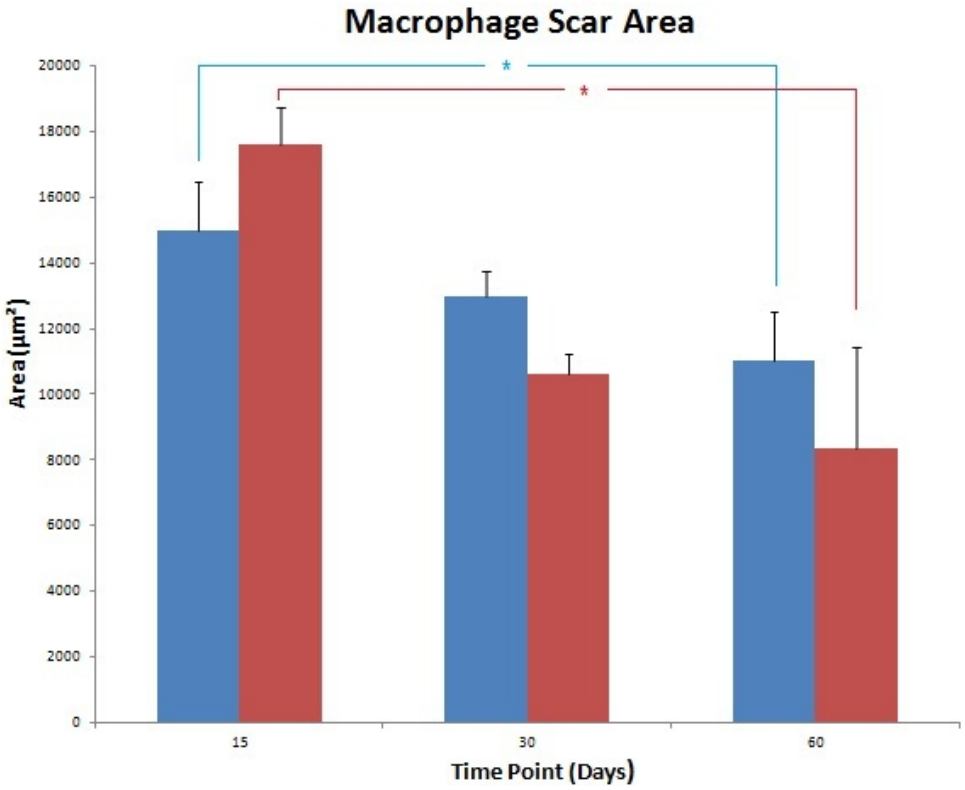

Figure 2-8 Progression macrophage scar area. Blue bars represent the acute model (Khobragade 2011) and red represent the subchronic model at 15 (n=4), 30 (n=4), and 60 (n=4) days post-implantation of REMI. (*) denotes a significant difference at $p < 0.05$ with one-way ANOVA followed with an Neuman-Keuls

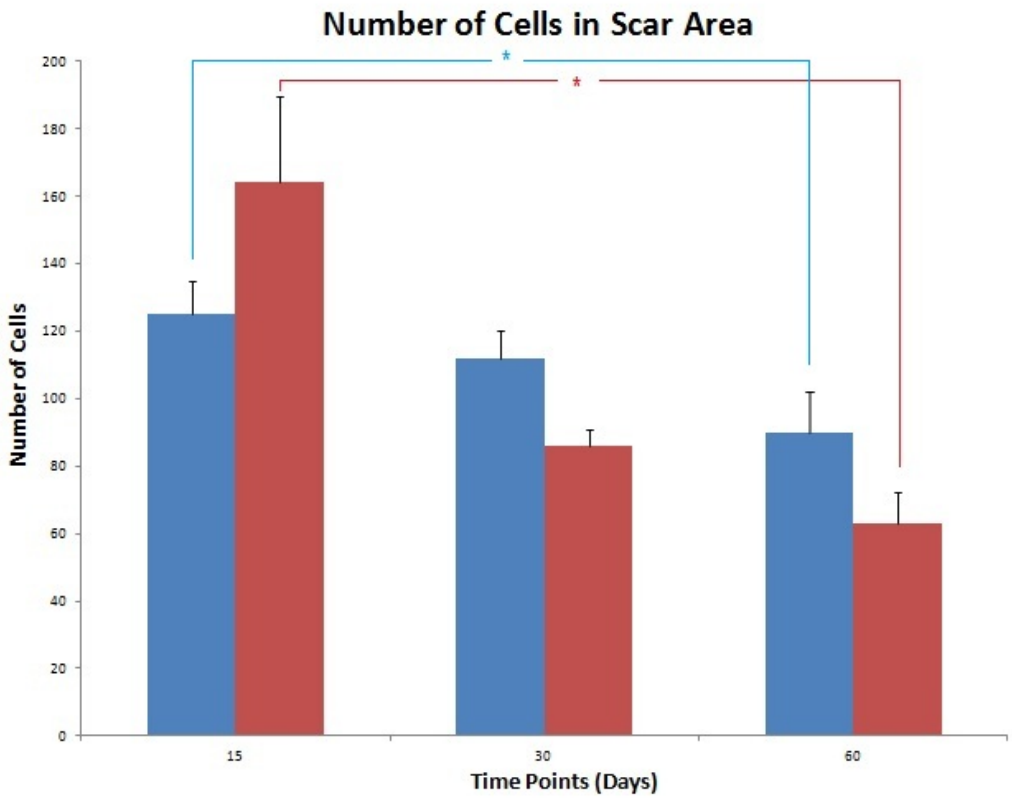

Figure 2-9 Progression of number of cells within scar. Blue bars represent the acute model (Khobragade 2011) and red represent the subchronic model at 15 (n=4), 30 (n=4), and 60 (n=4) days post-implantation of REMI. (*) denotes a significant difference at $p < 0.05$ with one-way ANOVA followed with an Neuman-Keuls

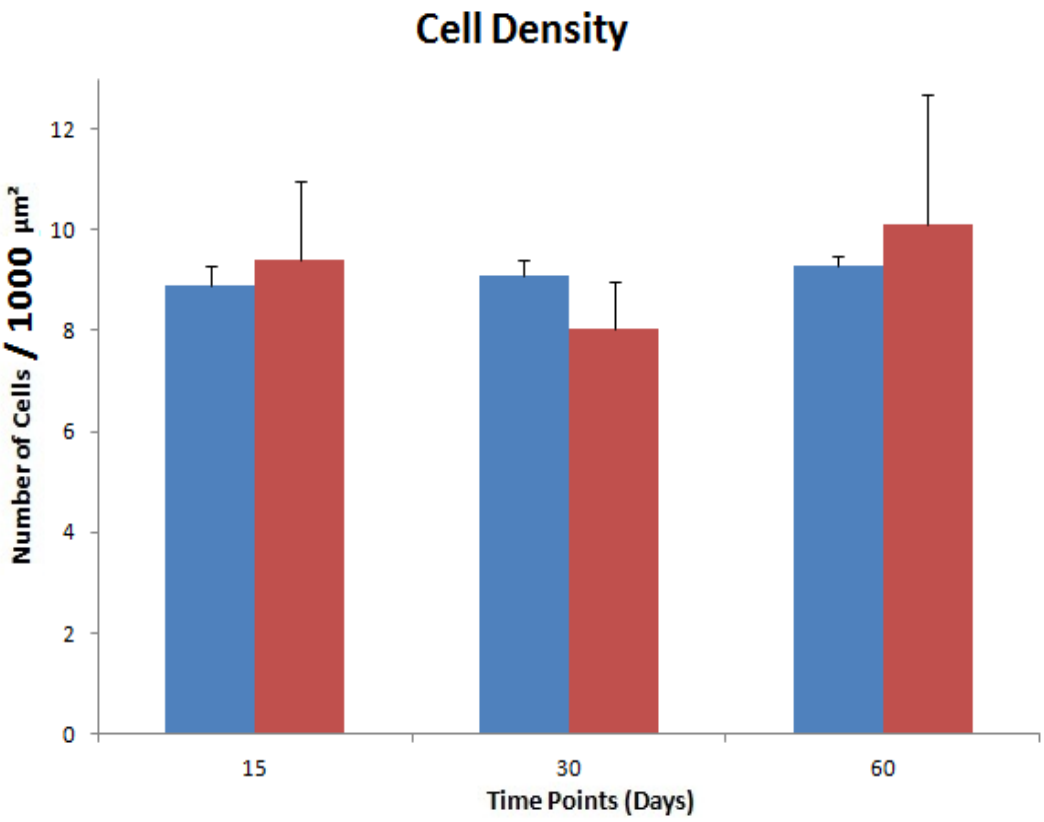

Figure 2-10 Progression of cell density within scar. Blue bars represent the acute model (Khobragade 2011) and red represent the subchronic model at 15 (n=4), 30 (n=4), and 60 (n=4) days post-implantation of REMI. (*) denotes a significant difference at $p < 0.05$ with one-way ANOVA followed with an Neuman-Keuls

Figure 2-8 quantitatively compares the macrophage scar area and figure 2-9 illustrates the number of cells found within the scar region due to electrode-tissue interfacing after 15, 30, and 60 days of implantation under acute and subchronic amputation conditions. A significant decrease was seen in the macrophage scare area and number of cells within the scar from 15-day to 60-day points post implantation for both, acute and subchronic amputated animals. Due to the decrease in scar area after 60 days, the cell density of the scare was measured to determine whether the scar had compacted. The graph in figure 2-10 shows the scar density at 15, 30, and 60 days

post-surgery for the acutely and subchronically implanted conditions. No significant difference in cell density was observed among any of the time times under either condition.

Discussion

The lack of reliability of multi-electrode arrays to interface the nervous system with a prosthetic limb over long periods of time have denied their use at the clinical level. Long term studies have reported a decline in the number of active channels after long-term amputations (Warwick, Gasson et al. 2003; Branner, Stein et al. 2004; Polikov, Tresco et al. 2005). Increased distance between electrode and action potential source (Salcman and Bak 1976; Polikov, Tresco et al. 2005) (placement of the electrode within 130 µm of an action potential source will, in theory, be observed below noise; while experimental data indicates that the electrodes should be no farther than 100 µm (Eaton and Henriquez 2005; Polikov, Tresco et al. 2005)), mechanical failures (breakage of electrodes and/or associated wiring) (Carter and Houk 1993), and neural plasticity (Darian-Smith and Gilbert 1994; Navarro, Vivó et al. 2007) have been postulated as possible explanation long-term interfacing failure. Our results show that in the sciatic nerve the distance between the electrode and the action potential source does not increase due to scar size; instead, it shows a significant reduction in scar size and foreign body response through the 15, 30, and 60 time points under acute and subchronic amputation. Further, there cell density within the scar, composed of ED1 reactive macrophages and fibroblasts (Lefurge, Goodall et al. 1991), show no significant difference through the three different time periods under either amputation condition. The data previously presented proves that 1) the scar around the REMI electrodes does not compact and 2) 30-day subchronic amputation does not affect the foreign body response in comparison to an acute amputation and implantation of the REMI. It is possible that the scar may play a role in the quality of signal obtained by the interfacing

electrode y increasing the distance between the action potential and electrode tip. Theoretical studies have calculated that the interfacing electrode should be no farther than 130 µm from the action potential in order to observe action potentials above noise. In actuality, experiments show that the required distance between electrode and action potential should not surpass 50 µm to 100 µm (Polikov, Tresco et al. 2005). Our experiments show that the scar size range from approximately 9000 μm^2 18000 μm^2 throughout the various time points, which corresponds to a radius of 54 µm to 75 µm, respectively. Rat macrophages are approximately 13 µm (Krombach, Münzing et al. 1997), which, if lined up, would require between 4 and 6 macrophages to create a scar with radii of 54 µm and 75 µm, respectively. Under extreme conditions, a scar size of 18000 μm^2 would not hinder signal acquisition if the distance limit is 100 µm; however, if the ideal distance limit is 50 µm, then there is a possibility that scar size alone will prevent the recording of action potentials. Likewise, a scar size of 9000 μm^2 would not prevent interfacing of tissue and electrode if the limiting distance is indeed 100 µm, but it would still create an obstacle if the limiting distance is 50 µm. However, because signals can still be recorded from the REMI even during highest macrophage recruitment (observed at 15 days, with a scar area of approximately 18000 μm^2 equaling to 75 µm in radius), it can be concluded that a limiting distance of 50 µm does not apply for interfacing the peripheral nervous system with the REMI. Thus, by utilizing extreme figures, this study shows that scar size may be a contributing factor for obtaining signals above noise but does not directly correlate with interfacing failure. Nonetheless, the direct correlation between decreasing scar size and progressive electrode interfacing failure (Nivedita, 2011) also point to other causes for the inability of long term interfacing. Figure 2-8 (A) illustrates the decrease in scar size through the 15, 30, and 60-day time periods, which directly correlates with the amount of failed electrode interfaces. Regardless of the scar size data directly correlating with the electrode failure trend, it cannot be regarded as an impediment to successful interfacing of the peripheral

nervous system. The scar size does, however, increase impedance of the REMI from approximately 300 kohm to 700 kohm (Dr. Romero, unpublished) most likely due to the presence of macrophages, fibroblasts and the formation of collagen around the electrodes (Lefurge, Goodall et al. 1991). The data also demonstrates that subchronic amputation and REMI implantation yields a comparable foreign body response as the acute model. To further enlighten electrode interfacing failure, different aspects relating to REMI implantation and nerve regeneration must be examined and evaluated. Chapter 3 will discuss the evaluation of nerve regeneration to obtain a superior evaluation of the impact, if any, of a subchronic amputation followed by an implantation of the REMI and Chapter 4 will discuss the possible effects of the blood-nerve barrier formation on the electrode signal acquisition.

Chapter 3

Evaluation of Nerve Regeneration

Background

Peripheral nerve regeneration involves interactions between cellular elements and the extracellular matrix. Axotomy causes the distal and proximal nerve stumps to retract, axoplasm leaks out and the membranes (epineurium, perineurium, endoneurium) collapse. Macrophages, recruited through cytokines, enhance the lysis and phagocytosis of the myelin and subsequent Schwann cell proliferation. In the distal nerve stump, the axonal and myelin degeneration, along with macrophage secretions stimulate the Schwann cells to proliferate within their basal lamina to form bands of Bungner to eventually form guiding conduits in order for the regenerating axons to reach their target site. Neurotrophic factors produced by Schwann cells in the distal stump enhance the nerve regeneration after injury. A second phase of Schwann cell proliferation, mediated by neurotrophic factors specific for glial cells, occurs when Schwann cells come into contact with the regenerating axons. If axonal regeneration is delayed, Schwann cell number decreases progressively and become less sensitive to axonal regeneration (Terenghi 2002). The fact that in these experiments the Lewis rats were subchronically amputated-- the distal stump was ligated with silk thread and the proximal stump sutured to the muscle (figure 2-2 A)--would indicate that poor nerve regeneration is expected. However, during regeneration the proximal stump axons give rise to neuronal sprouts which theoretically maximize the chances for each neuron to reach its target organ (Wong and Mattox 1991). Moreover, the proximal stump was deliberately sutured to the biceps femoris to facilitate the process of the proximal regenerating axons to reach and reinnervate their target site and help prevent further degeneration of the proximal nerve stump.

Peripheral nerve regeneration after acute amputation was previously evaluated in our laboratory; shown in figure 3-1, 3-2, and 3-3. However, peripheral nerve regeneration after a 30-day subchronic amputation has not been studied in terms of progressive axonal growth and remyelination, which this study aims to investigate through the makers Protein Zero (P0) and Neurofilament 200 (NF200). Anti-P0 antibody recognizes P0, the major glycoprotein in the peripheral myelin. Anti-NF200 antibody recognizes one of the three neuron-specific proteins in neurofilaments. The three groups of animal samples(15, 30, and 60 days post-REMI implantation) were immunolabled for P0 and NF200 and the extent of axonal regeneration and remyelination were studied and compared to animals implanted after an acute amputation.

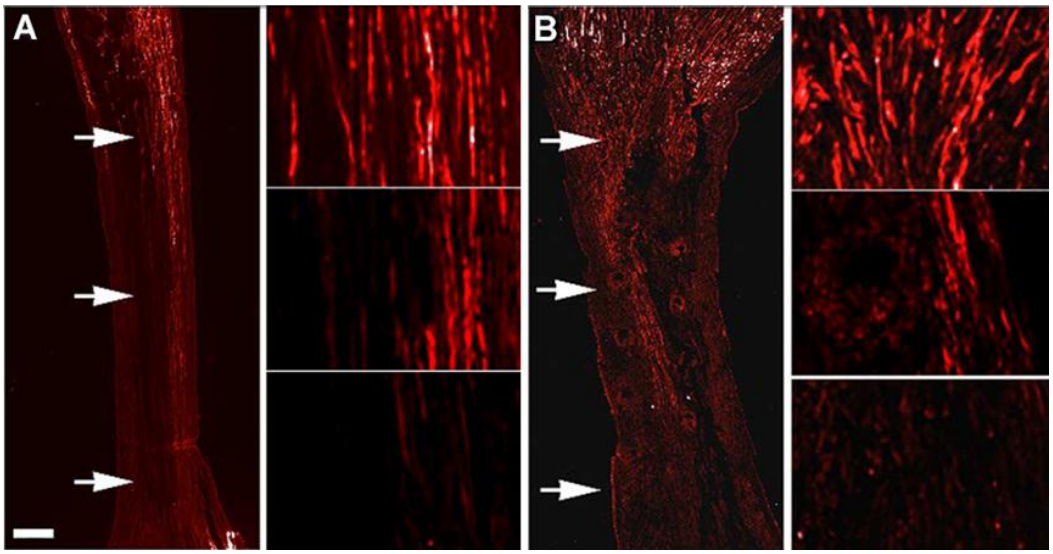

Figure 3-1 Immunolabeling of regenerated nerve tissue with P0. Image A and B show partial remyelinization at 15 days post REMI or control implantation. The arrows indicate areas which have been magnified to the right of each respective photograph. Scale bars = 200 µm (image A and B), 35 µm (smaller inserts) (adapted from (Seifert, Desai et al. 2011))

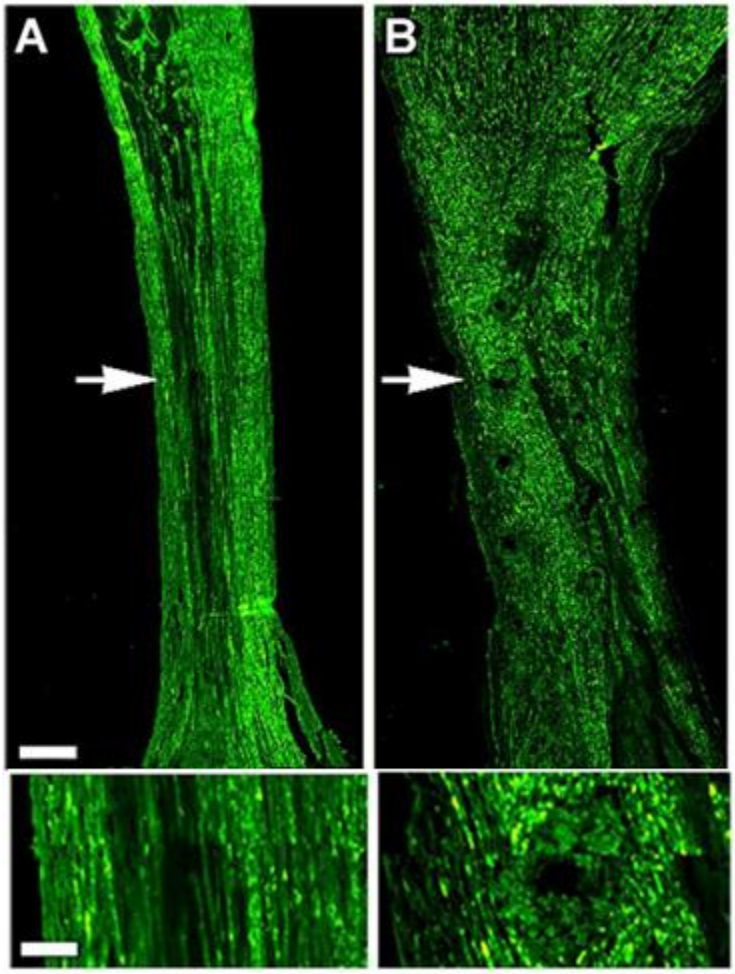

Figure 3-2 Immunolabeling of regenerated nerve tissue using NF200: 15 days post repair using either a simple tube (A) or a REMI (B). Image A and B show comparable axonal growth across the nerve gap (~5 mm). The arrows indicate areas of high magnification in their respective lower photographs. Scale bars = 200 µm (top), 55 µm (bottom) (adapted from (Seifert, Desai et al. 2011))

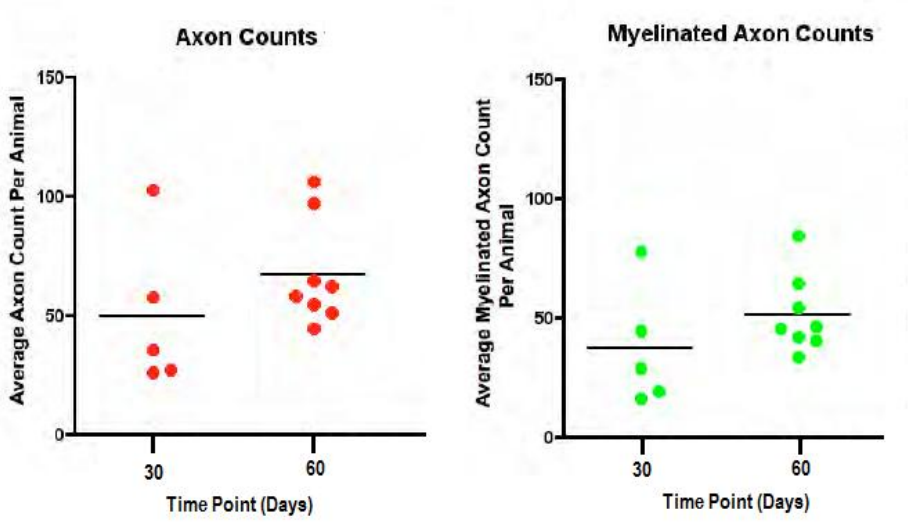

Figure 3-3 Quantification of total number of axons and of myelinated axons of acutely implanted REMI. Each data point represents average number of axons or myelinated axons at proximal, middle, and distal region of each nerve sample (Watson 2012). Refer to Imaging and Quantification methods of Chapter 3 for more detailed explanation

Methods

Immunofluorescence Staining

The sectioned and mounted nerve tissue samples were placed in an oven at 58-60˚ Celsius for 30 minutes to facilitate the attachment of tissue and to soften the paraffin. The tissues were then rehydrated in by placing them in two baths of xylem for five minutes each, followed by two baths of 100% EtOH for three minutes each, then one bath of 90% EtOH for three minutes, then one bath of 70% EtOH for 3 minutes, and finally a bath in DI water for 10 seconds. Epitope retrieval was accomplished with a citric acid bath at 80-85˚ Celsius for 15 minutes. Then the citric acid bath was allowed to continue for another 20 minutes at room temperature. A three-minute DI water bath was performed and then two baths with 1X PBS for 5 minutes on orbital shaker. The slides were dried and hydrophobically marked to prevent the primary and secondary solutions

to escape the slide. 500 µL of blocking solution (4% normal goat serum (NGS), 0.5% Triton X in 1X PBS) was added to each slide for one hour. Then three baths of washing solution (1X PBS and 0.5% Triton X) for 15 minutes each were performed. Finally, the primary antibodies were added (chicken anti-P0, Millipore, 1:200 dilution rate and rabbit anti-NF200, Sigma, 1:200 dilution rate). Twelve hours later, the samples were washed three times with washing solution for 15 minutes each, and once with 1X PBS for 15 minutes. The secondary staining (IgG Dylight 488, 1:400 dilution rate) in washing solution was then performed and incubated for one hour. The samples were washed three times with washing solution for 15 minutes each, and once with 1X PBS for 15 minutes. The slides were then mounted for Confocal/fluorescent microscope studies.

Imaging and Quantification

Images of the sciatic nerve obtained post the immunohistochemistry procedure using a ZEISS Observer Z1 fluorescent microscope with an automated stage, which allowed photographing the entire nerve regenerate.

The nerve tissue sample photographs were analyzed using ImageJ Software. A line was super imposed across the proximal, middle, and distal regions of the regenerate and the number of axons (NF200+ signal) and remyelinated axons (NF200+ & P0+ signal) was quantified at each line; the process is illustrated in figure 3-4. The averages at each region of the regenerated were obtained using the AVG function in MS EXCEL. The results were then statistically analyzed and compared among the time periods for the sub-chronic animals and previous results with acutely amputated animals.

Statistical analysis

The extent of nerve regeneration and remyelination for the subchronic results were compared to their corresponding region (e.g., proximal regions at 15, 30, and 60

days) to determine the existence of a significant difference using one-way ANOVA followed by Neuman-Keuls comparison *post hoc* evaluation (Prism 6, Graphpad). P-values less than 0.05 were considered statistically significant. The results were reported as mean ± standard error of the mean.

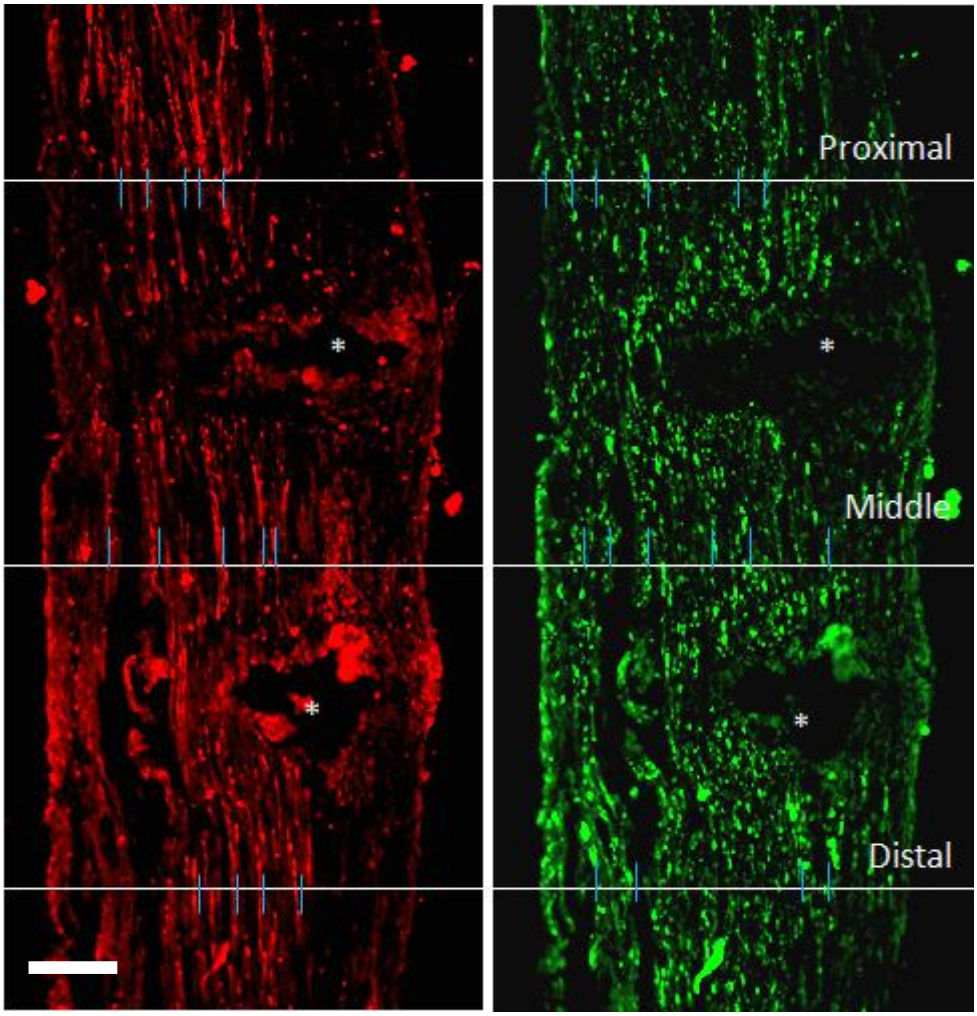

Figure 3-4 Axon and remyelination quantification. Graphical representation of remyelinated axons (P0+ signal, red) and axon (NF200+ signal, green) quantification. Blue lines crossing the white lines at the proximal, middle, and distal regions represent either an axon or remyelinated axon at that region. Asterisks (*) denote the region of explanted electrode shafts. Scale bar; 100 µm

Results

Previous studies from our laboratory have documented that under acute amputation conditions the REMI does not affect the regenerative extent of the sciatic nerve; at 15 day time period post-acute amputation, the regenerated nerve compares to the control in terms of axonal regeneration and remyelination (Seifert, Desai et al. 2011). Remyelination at 15 days after injury was not complete (figure 3-2); the distribution of P0-positive axons is more abundant towards the proximal end of the nerve, and diminishes in the middle of the nerve sample (figure 3-2). This pattern confirms the immaturity of the regenerated nerve after 15 days of REMI or control implant under acute amputation conditions.

The pattern of remyelinated axons under subchronic amputation conditions approximately matches the results under acute amputation conditions at 15 days post-implantation. Also, there is a significant difference in the number of axons regenerated (NF200+ signal) among the corresponding proximal, middle, and distal regions at the 15 and 60-day time periods. Likewise, there is a significant difference in the number of remyelinated axons (P0+ signal) among the corresponding proximal, middle, and distal regions at the 15 and 60-day time periods. Figure 3-8 summarizes the results of axonal regeneration and remyelination studies. The axonal regeneration pattern shown in figure 3-8 is supportive of the ability of peripheral nerve to regenerate post-subchronic amputation. However, in comparison to the results shown in figure 3-3, the average regenerated axons and remyelinated axons for the subchronic model are significantly less at 30 and 60 day time points. The average regenerated axons count for acute and subchronic model at 30 and 60 day time points were approximately 50, 65, 14, and 27, respectively. The average remyelinated axon count for acute and subchronic at 30 and 60 day time points were approximately 40, 55, 12 and 27, respectively. Also, at time point 15 and 30, there is a negative trend from proximal to middle to distal region for the

axon count and remyelination count. By day 60 both, axonal regeneration and remyelination of the proximal, middle, and distal show no defined trend. Comparisons among proximal, middle, and distal regions at each time period for both NF200 and P0 immunostainings revealed no statistical significance.

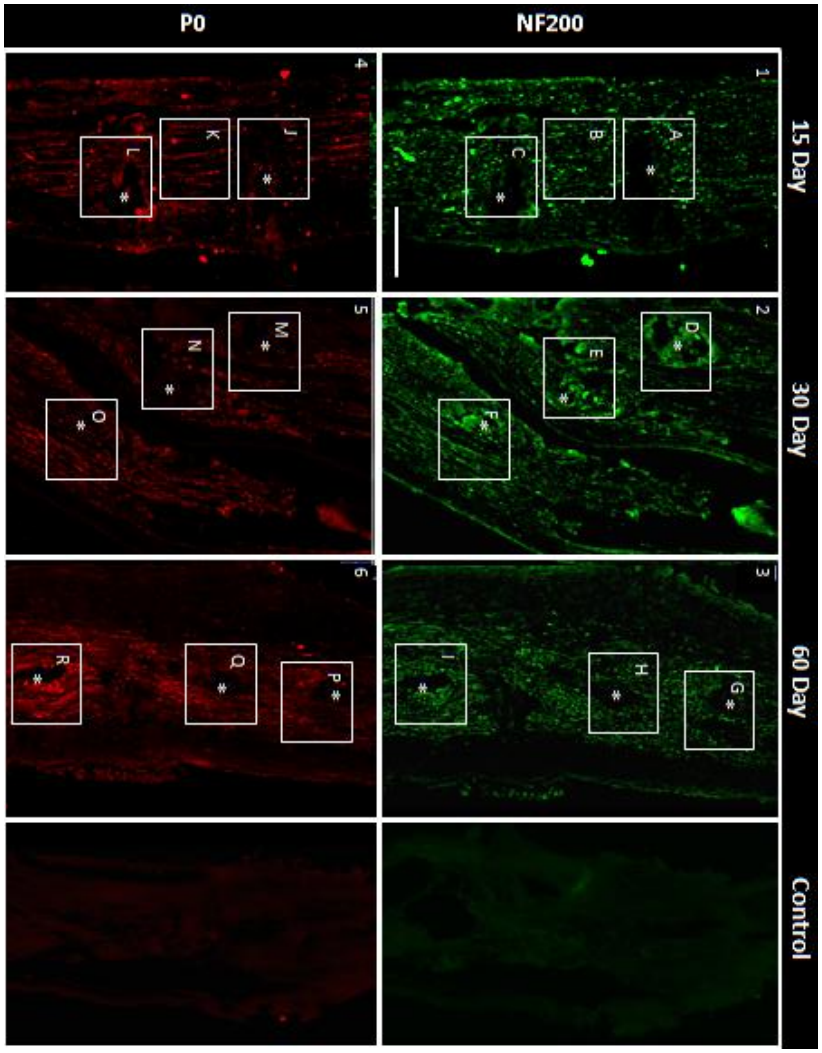

Figure 3-5 Representation of axon and remyelinated axon progression for subchronically amputated animals.Asterisks (*) denote explanted electrode region. White boxes are shown at higher magnification In figure 3-5 to 3-6. Scale bar; 250 µm

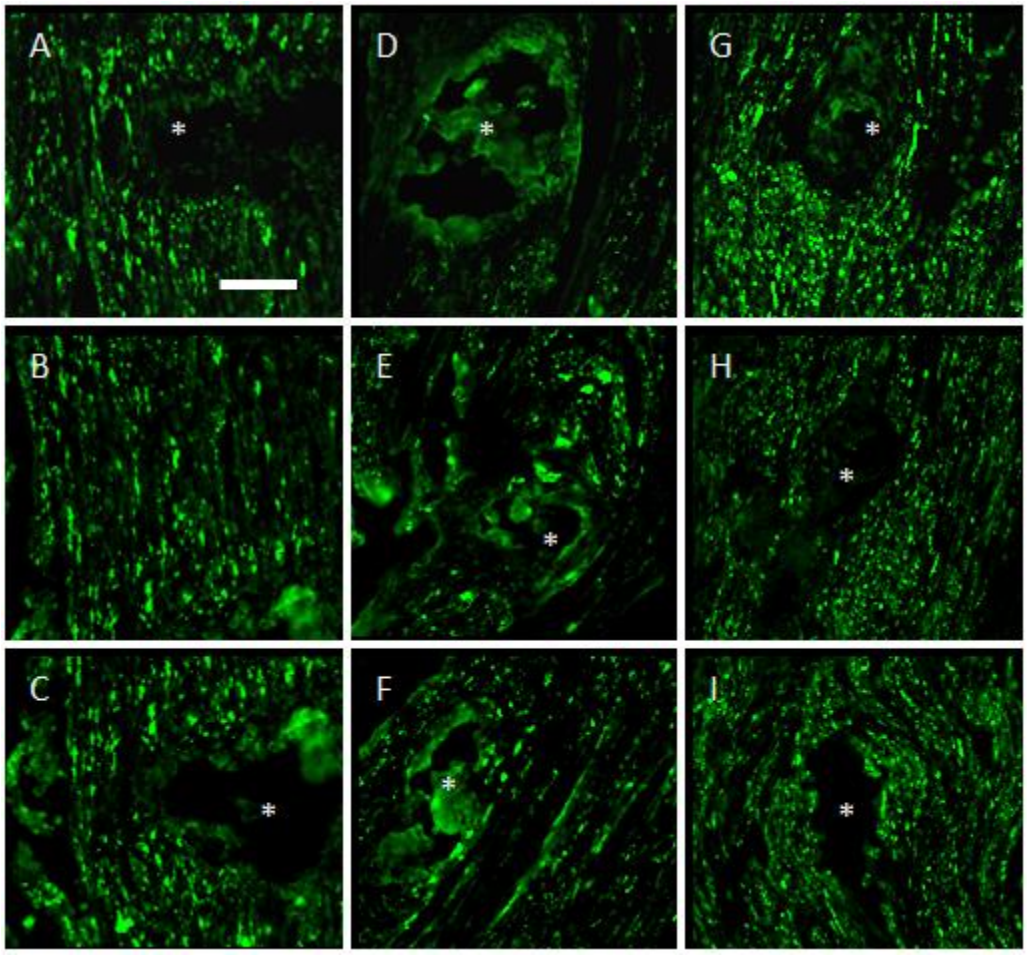

Figure 3-6 Magnified view of white boxes in figure 3-5 A-I. NF200+ signals are shown under higher magnification to show more detail of the immunolabeled axons. Scale bar 60 µm

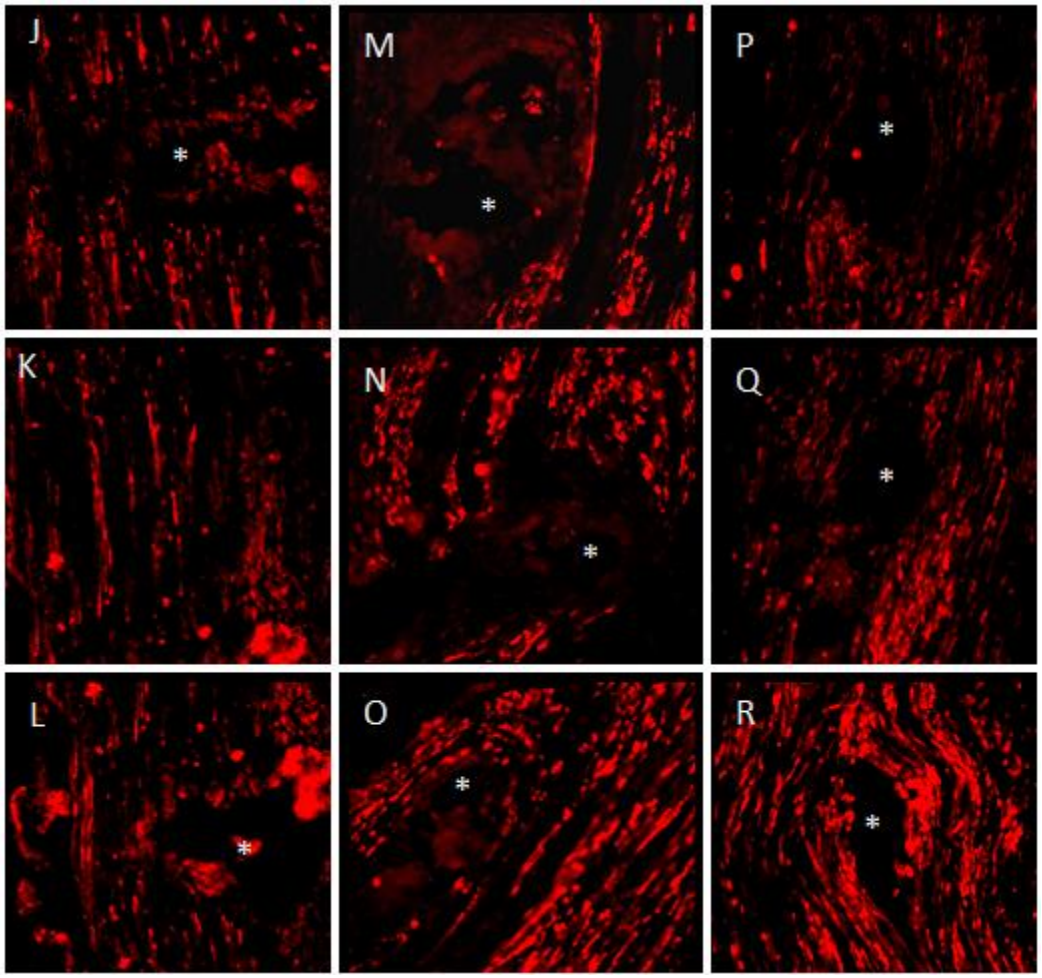

Figure 3-7 Magnified view of white boxes in figure 3-5 J-R. P0+ signals are shown under higher magnification to show more detail of the immunolabeled axons. Scale bar 60 µm

.

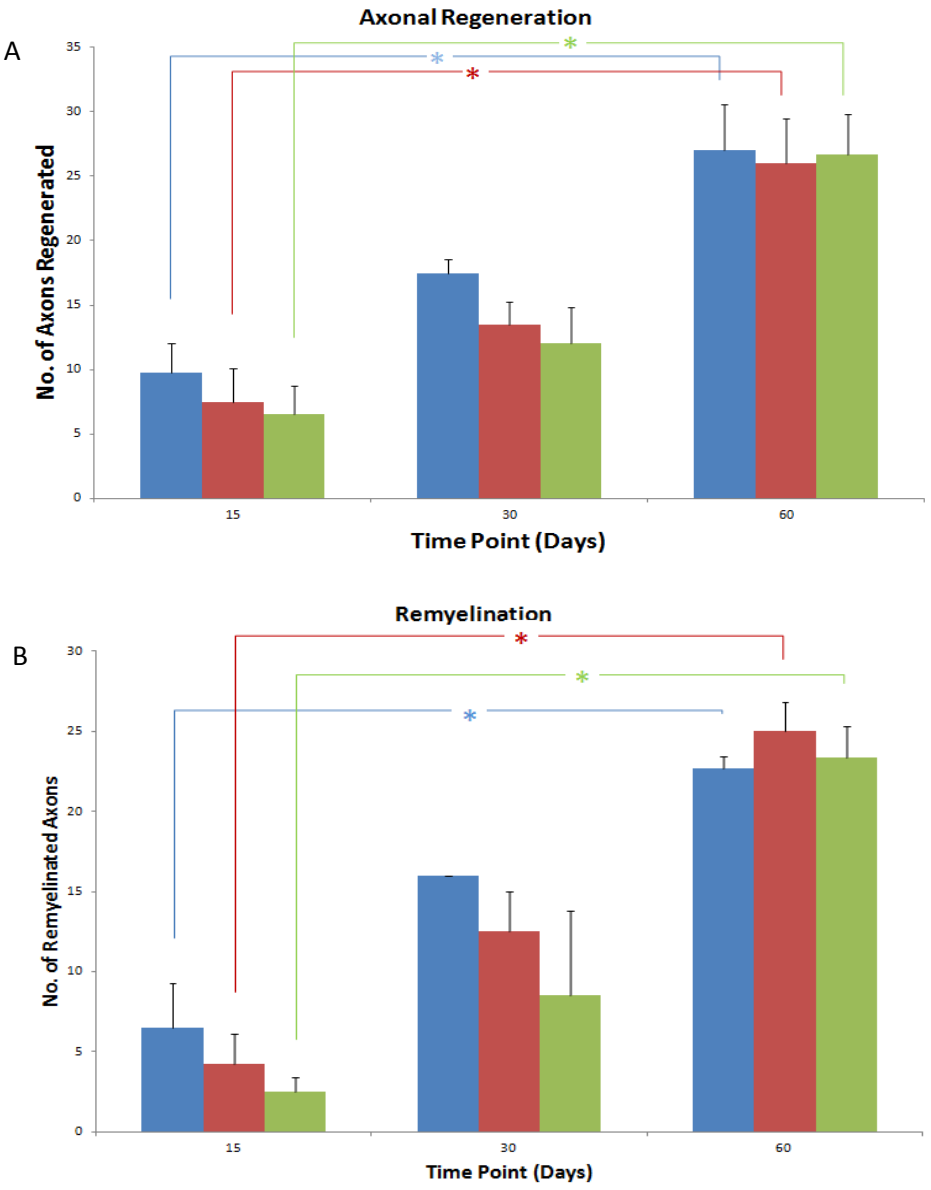

Figure 3-8 Regenerated axons (A) and remyelination results (B). Each time point (15 (n=4), 30 (n=2), and 60 (n=4) days) shows information for the number of axons/remyelinated axons at the proximal (blue), middle region (red), and distal (green) region. Asterisks (*) denote a significant difference using ANOVA test followed by Neuman-Keuls comparison test; p-Values < 0.05 were considered significant

Discussion

As expected, the axonal regeneration extent and remyelination are the least after 15 days of REMI implantation and significantly increase 45 days subsequently. The data shows a positive trend in terms of overall axonal regeneration and remyelination. No significant difference are found among the proximal, middle, and distal region at each time point for either number of axons regenerated or number of axons remyelinated, which leads to the assumption that complete nerve regeneration takes at least 15 days. Figure 3-8 shows that as time progresses through the three different time points, the difference in axonal regeneration and remyelination among the proximal, middle, and distal regions becomes less pronounced. At 15 and 30 day time points for number or axons regenerated and remyelinated axons, the decreasing pattern from proximal to middle to distal region further solidifies the well-known fact that peripheral nerve regenerates from proximal to distal direction (Faweett and Keynes 1990) . Figure 3-8 data demonstrates that nerve regeneration in terms of axon number and remyelination is increasingly progressive; however, it does not regenerate to the same extent after 30 and 60 days as the acute model shows in figure 3-3. Results obtained for the subchronic amputation model do not yield comparable results in terms number of axons regenerated or remyelination in comparison to the acute amputation model. The average regenerated axons and remyelinated axons for the subchronic model are significantly less at 30 and 60 day time points. The average regenerated axons count for acute and subchronic model at 30 and 60 day time points were approximately 50, 65, 14, and 27, respectively. The average remyelinated axon count for acute and subchronic at 30 and 60 day time points were approximately 40, 55, 12 and 27, respectively. These results do not support previous research where a crushing priming injury 2 weeks prior to nerve excision resulted in a 27% increased rate of sciatic nerve elongation in adult mice (McQuarrie and Grafstein 1973). However, for our subchronic model, the priming injury was a complete sciatic nerve transection 30 days prior to the second injury—REMI

implantation. A one month time lapse between priming injury and second injury could be enough time to result in the down-regulation of stress factors initiated by the first injury (Leon, Yin et al. 2000), thus eliminating the positive effects of a priming injury. Remyelination of peripheral nerve fibers restores the normal security and signal conduction at near normal velocity (Smith and Hall 1980). The data collected shows that remyelination starts no later than 15 days post injury and continues up to 30 days, with practically complete myelin sheath formation at 60 days. Electrode interfacing failure as time progresses (shown in figure 1-7) does not correlate with the trends shown in figure 3-8, where remyelination occurs and thus normal security and signal conduction returns at near pre-injury velocity. As the axons become functional and able to transmit signals, the quantity and quality of the action potential signal acquisition increases; however, after remyelination is complete and the axons have achieved a near-healthy state, the interface begin to fail regardless. Initially, there is a direct correlation among axon count or axon remyelination and percentage of active channels. After 21 days, the correlation among axon count or axon remyelination, and percentage of active channels becomes indirect. Thus, it can be concluded that subchronic amputation produces a similar initial nerve regeneration growth pattern, but does not regenerate to the same extent as nerves which have been interfaced post acute amputations. Results obtained thus far, however, are not sufficient to explain the electrode signal acquisition failure explained in figure 1-7. Hence, Chapter 4 explores and evaluates the integrity of the blood-nerve barrier and tight junction formation in relation to electrode interfacing failure over extended periods of time.

Chapter 4

Integrity of Blood Nerve Barrier

Background

The blood nerve barrier (BNB) is a functional barrier between the peripheral nervous system and the circulatory system (Poduslo, Curran et al. 1994). The BNB is composed of endoneurial microvasculature and other inner layers of the perineurium. Tight junctions (TJs) between adjacent peripheral nerve microvascular endothelial cells (PnMECs) are responsible for BNB function (Kashiwamura, Sano et al. 2011). Further, myelinating Schwann cells are responsible for the formation autotypic junctions in the Schmidt Lanternman incisures, paranodal loops, mesaxons and the outer aspect of the nodal gap. Direct physical injury to the peripheral nerve has demonstrated an increase in perineurial permeability to proteins at the site of lesion. Wallerian degeneration at the distal nerve stump post nerve injury (acute trauma or transection) has been well documented; this event is associated with endoneurial edema, which leads to a progressive increase in fluid pressure (4 to 5 times the normal pressure) within the first week following the injury. Alteration in the permeability properties of the endoneurial blood vessels have been linked to nerve edema in the Wallerian degeneration; increased permeability to blood serum protein in nerve capillaries has been previously demonstrated. Furthermore, studies have shown, that except in the immediate vicinity of nerve trauma, the perineurium retains its integrity in the degenerating nerve stump (Rechthand and Rapoport 1987). Even under healthy conditions, the BNB is semi-permeable to peptides and proteins; transport mechanisms postulated include (i) transmemebrane diffusion, (ii) carrier-mediated transport, (iii) fluid-phase endocytosis, (iv) nonspecific adsorptive endocytosis, and (v) specific or receptor-mediated adsorptive endocytosis. Ion (Poduslo, Curran et al. 1994); thus free diffusion through the BNB does not occur. The effect of the BNB on the Pt/Ir-electrode signal recording is extremely

relevant. We have hypothesized that the formation of the BNB around the implanted electrodes directly contributes to lead failure. Figure 4-1 summarizes our proposed mechanism leading to failure of electrodes to record action potentials from nearby axons. Thus Chapter 4 examines the TJ structure formation as the nerve regenerates though the REMI and the possibility that such formation could affect the ion diffusion and signal acquisition from the electrodes.

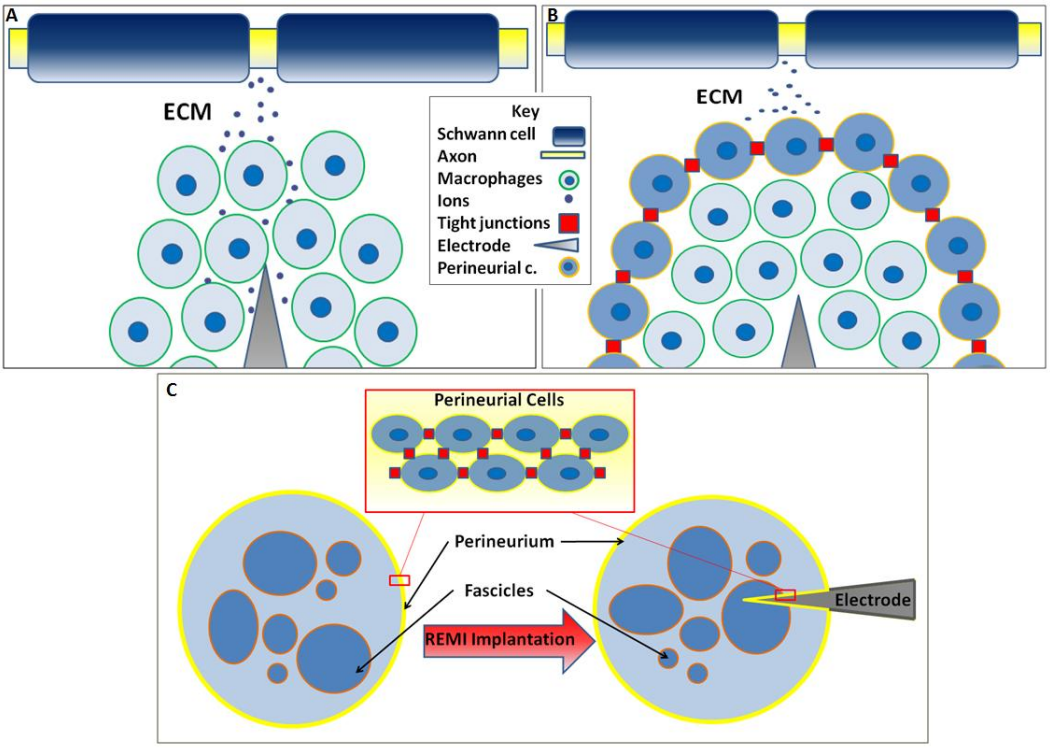

Figure 4-1 Conceptual illustration of known initial mechanism (A) and hypothesized mechanism (B-C) leading to interfacing failure. A) Signal recording possible despite foreign body response leading to scar formation. B) proposed mechanism for electrode lead failure as time progresses: following foreign body response, perineurial cells of the BNB form around the scar leading to electrode acquisition signal. C) Cross-sectional view of the peripheral nerve before and proposed perineurium formation around electrodes post REMI implantation.

Claudin-1, a member of at least 24-member claudin family, is a small tetraspan membrane protein with two short extracellular loops and short cytoplasmic N- and C-termini. Claudins play a crucial role in the formation of the BNB barrier in peripheral nerve by homotypically and heterotypically adhering Perineurial cells to each other (Pummi, Heape et al. 2004). In this chapter, the integrity of the BNB was evaluated after acute and subchronic amputation for three different time points: 15, 30, and 60 day post REMI implantation. Anti-Claudin-1 antibody was used to immunolabel parts of the TJ structure and anti-ED1 antibody was used to mark macrophages. Through the use of confocal microscopy and immunohistochemistry, the BNB regeneration in relation to scar formation was investigated to see if there was a relation with the regeneration of the BNB and the failure of the electrode interfaces. Furthermore, the BNB regeneration integrity was compared under acute and subchronic amputation conditions.

Methods

Immunofluorescence Staining

The sectioned and mounted nerve tissue samples were placed in an oven at 58-60˚ Celsius for 30 minutes to facilitate the attachment of tissue and to soften the paraffin. The tissues were then rehydrated in by placing them in two baths of xylem for five minutes each, followed by two baths of 100% EtOH for three minutes each, then one bath of 90% EtOH for three minutes, then one bath of 70% EtOH for 3 minutes, and finally a bath in DI water for 10 seconds. Epitope retrieval was accomplished with protease (Sigma P-5147) at 1-2mg/ml for 10 minutes at 37˚C. The slides were dried and hydrophobically marked to prevent the primary and secondary solutions to escape the slide. 500 µL of blocking solution (4% normal goat serum (NGS), 0.5% Triton X in 1X PBS) was added to each slide for one hour. Then three baths of washing solution (1X PBS and 0.5% Triton X) for 15 minutes each were performed. Finally, the primary antibodies were added (rabbit anti-Claudin-1, Life Technologies, 8 mg/mL dilution rate

and mouse anti-ED1, Millipore, 1:250 dilution rate). Twelve hours later, the samples were washed three times with washing solution for 15 minutes each, and once with 1X PBS for 15 minutes. The secondary staining (Goat anti Mouse IgG Dylight 488, 1:400 dilution rate and Goat and Rabbit IgG Dylight 594, 1:500 dilution rate) in washing solution was then performed and incubated for one hour. The samples were washed two times with washing solution and then a counter-stain of TO-PRO-III (1:500 dilution rate) was performed. Two more washes with washing solution for 15 minutes each, and once with 1X PBS for 15 minutes. The slides were then mounted for Confocal/fluorescent microscope studies.

Imaging and Quantification

Pictures were taken of the sciatic nerve post-immunohistochemistry steps using a Confocal microscope (Zeiss LSM 510) with three single photon lasers (Ar, HeNe 543, HeNe 633) which allow the user to select lines of 458, 488, 514, 543, 568, and 633 nm. For our purposes, the filters were set up to allow lines of 488 and 568 to visualize the anti-mouse DyLight 488 secondary antibody (mouse anti-ED1 primary) and Dylight 594 secondary antibody (rabbit anti-Claudin-1 primary).

The photographs were analyzed using ImageJ Software. A rectangle with the dimensions equal to that of the thickness of the scar was placed within the scar region and a rectangle of the same dimensions was placed adjacent to the scar. Then, the gray value of the selection was measured. This is the sum of the gray values of all the pixels in the selection divided by the number of pixels; reported in calibrated units (e.g., optical density). This procedure measured the intensity of the red and green pixel signal, which represented the anti-rabbit Dylight 594 (bound to rabbit anti-claudin-1) and anti-mouse Dylight 488 (bound to mouse anti ED1) antibodies, respectively. The x-axis represents the horizontal distance through the selection and the y-axis the vertically averaged pixel intensity. This process (figure 4-2) was performed four times around each electrode scar

(four rectangles within the scar and four rectangles of identical size adjacent to the scar). Four scars per animal were analyzed. The averages were obtained using the AVG function in MS EXCEL.

Statistical analysis

The extent of TJ formation under acute and subchronic amputation was compared using paired student's t-test for unequal variances between the inside and outside of the scar region. A significance level of $\alpha = 0.05$, p-values less than 0.05 were designated to be statistically significant. The results were reported as mean ± standard error of the mean. For multiple-group comparison, one-way ANOVA followed by Neuman-Keuls comparison *post hoc* evaluation (Prism 6, Graphpad). P-values less than 0.05 were considered statistically significant. The results were reported as mean ± standard error of the mean.

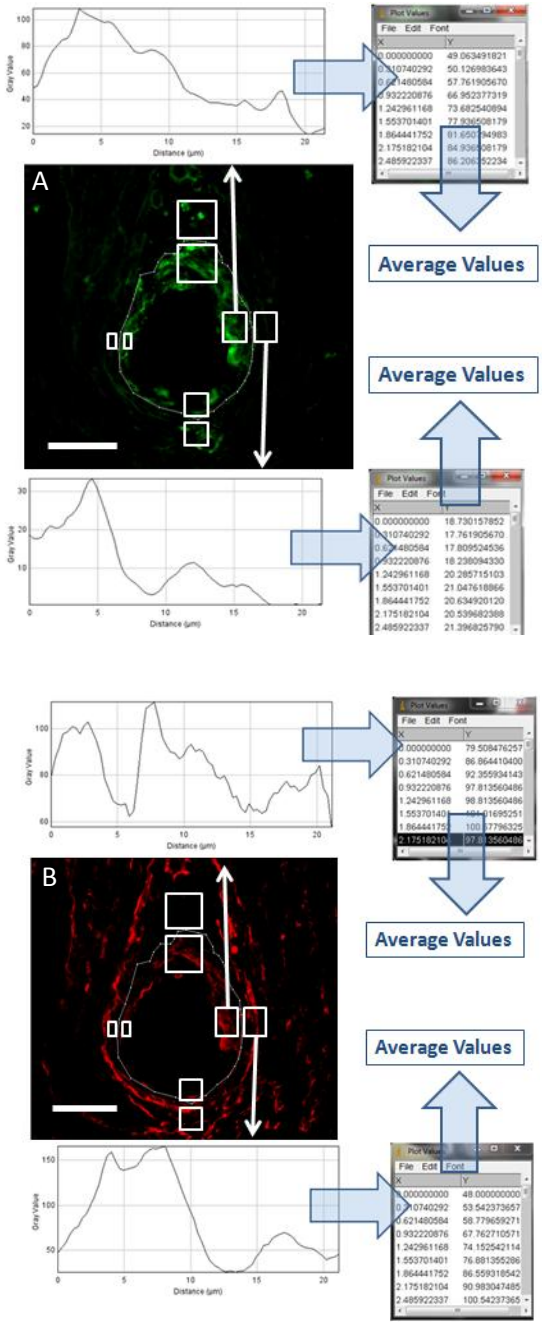

Figure 4-2 Methods for ED1(A) and Claudin-1 quantification (B). The method was performed four times within the scar and four times adjacent to the scar. The gray values (optical densitometry) within the scar were averaged and plotted; gray values adjacent to the scar were averaged and plotted. Gray values were obtained from the gray value profile plot. White line marks scar region. Scale bar; 70 μm

Results

The ED1 optical densitometry analysis showed no significant difference in the signal between the inside and outside of the scar at each time period for the acutely and chronically amputated conditions nerve samples. Optical densitometry analysis showed no significant difference in the Claudin-1 signal between the inside and outside of the scar at each of the time periods for the subchronically amputated condition nerve samples. Multi-group comparisons revealed no statistical differences among the progressive values (15, 30, and 60-day time points) inside the scar for acute/subchronic conditions of ED1 quantification; also, no significant difference was observed outside the scar for acute/subchronic conditions of Claudin-1 quantification. However, there was a progressive pattern for both of the amputation models: as time progressed, the intensity of Claudin-1 signal decreased in comparison with the Claudin-1 signal intensity immediately outside of the scar until the optical densitometry value was greater outside of the scar than inside at 60 days post REMI implantation. In other words, there was an apparent reduction in concentration of TJs within the scar while an increase in concentration and more organized pattern of TJ outside of the scar, as shown in figures 4-3 and 4-4. Figure 4-3 quantitatively shows the expected results for ED1 for acute and subchronic amputation conditions: higher densitometry values within the scar compared to the area outside of the scar. Claudin-1 densitometry values are greater within the scar area at 15 days, at 30 days these values were approximately equal, and at 60 days the intensity of the Claudin-1 signal was greater outside of the scar than inside. This pattern is qualitatively represented by figure 4-4, which shows the sciatic nerve samples immunolabeled with Claudin-1, ED1, and TO-PRO-3.

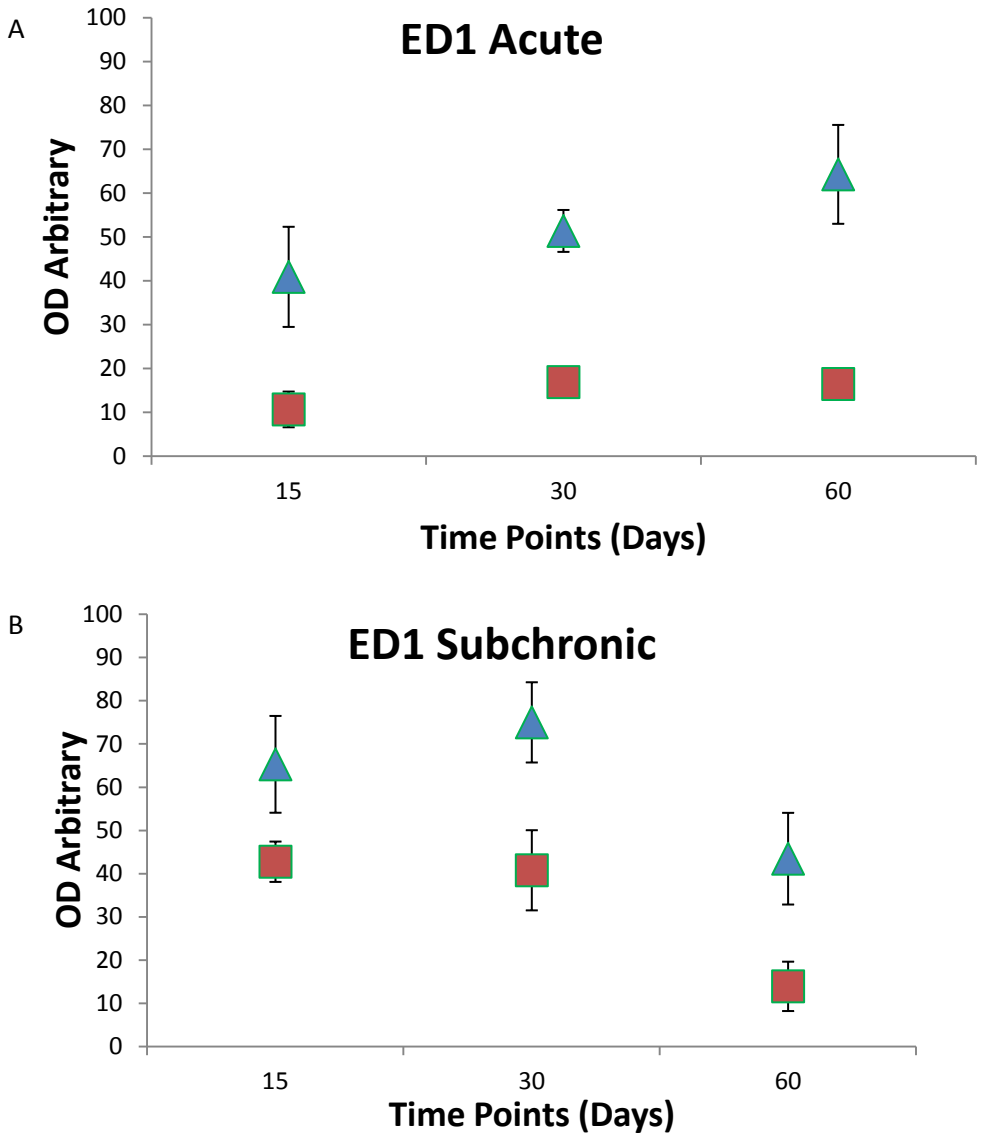

Figure 4-3 Optical densitometry results for ED1 for acute (A) and subchronic (B) models. Values within (blue triangle) and outside (red square) the scar are shown at 15 (n=4), 30 (n=4), and 60 (n=4) days after REMI implantation. Asterisks (*) denote a significant difference using ANOVA test followed by Neuman-Keuls comparison test; p-Values < 0.05 were considered significant

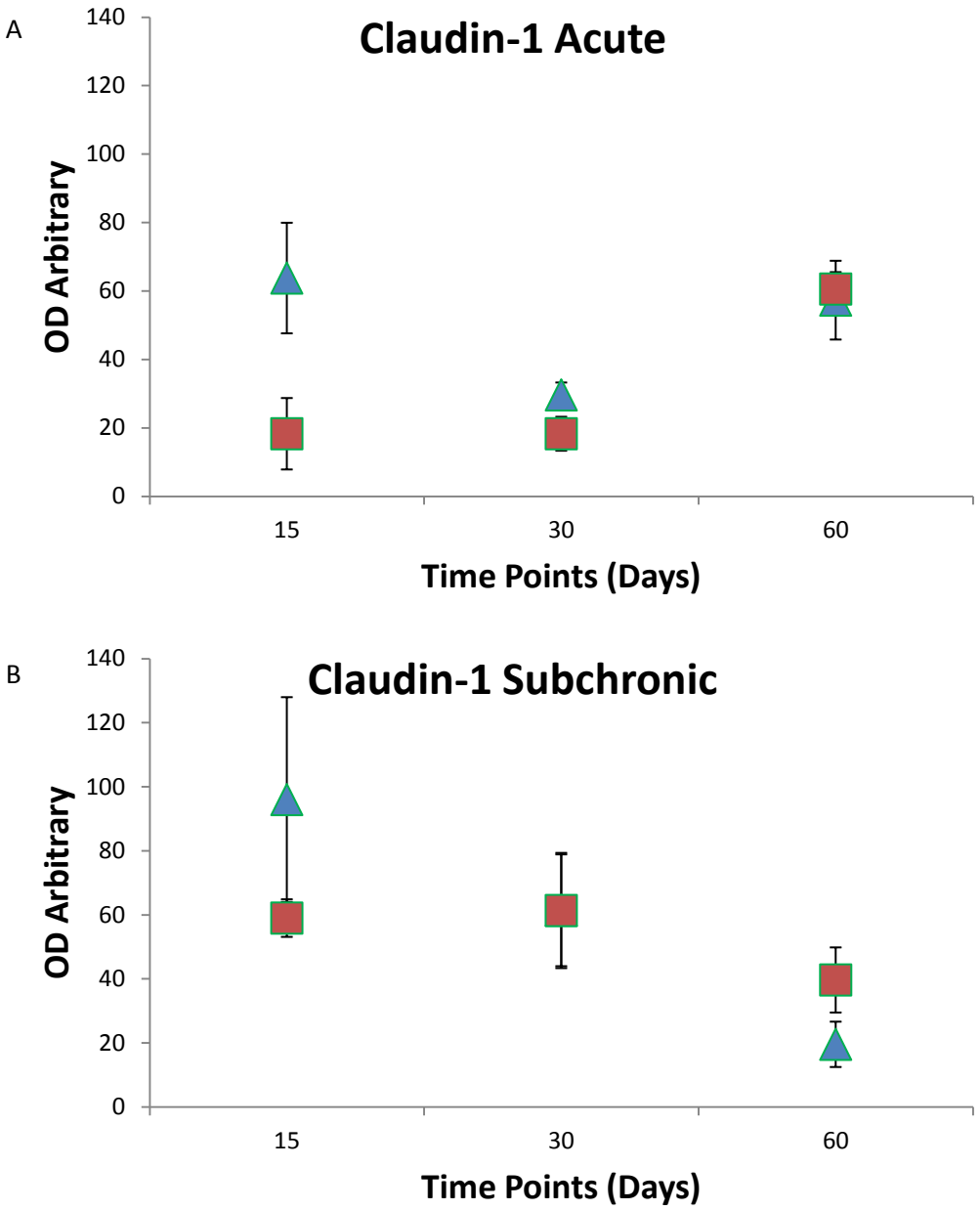

Figure 4-4 Optical densitometry results for Claudin-1 for acute (A) and subchronic (B) models. Values within (blue triangle) and outside (red square) the scar are shown at 15 (n=4), 30 (n=4), and 60 (n=4) days after REMI implantation. Asterisks (*) denote a significant difference using ANOVA test followed by Neuman-Keuls comparison test; p-Values < 0.05 were considered significant

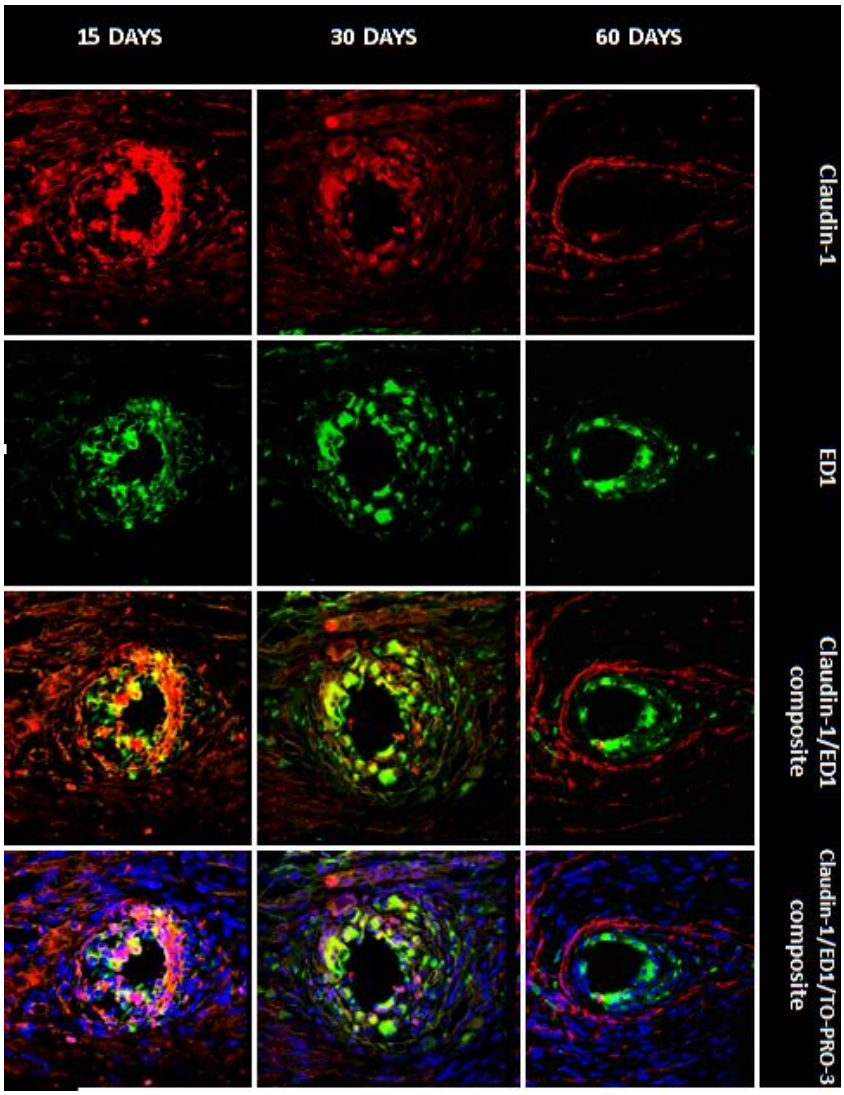

Figure 4-5 Immunolabeling nerve tissue with Claudin-1, ED1, and TO-PRO-3 of acute amputation model. Scale bar; 50 μm

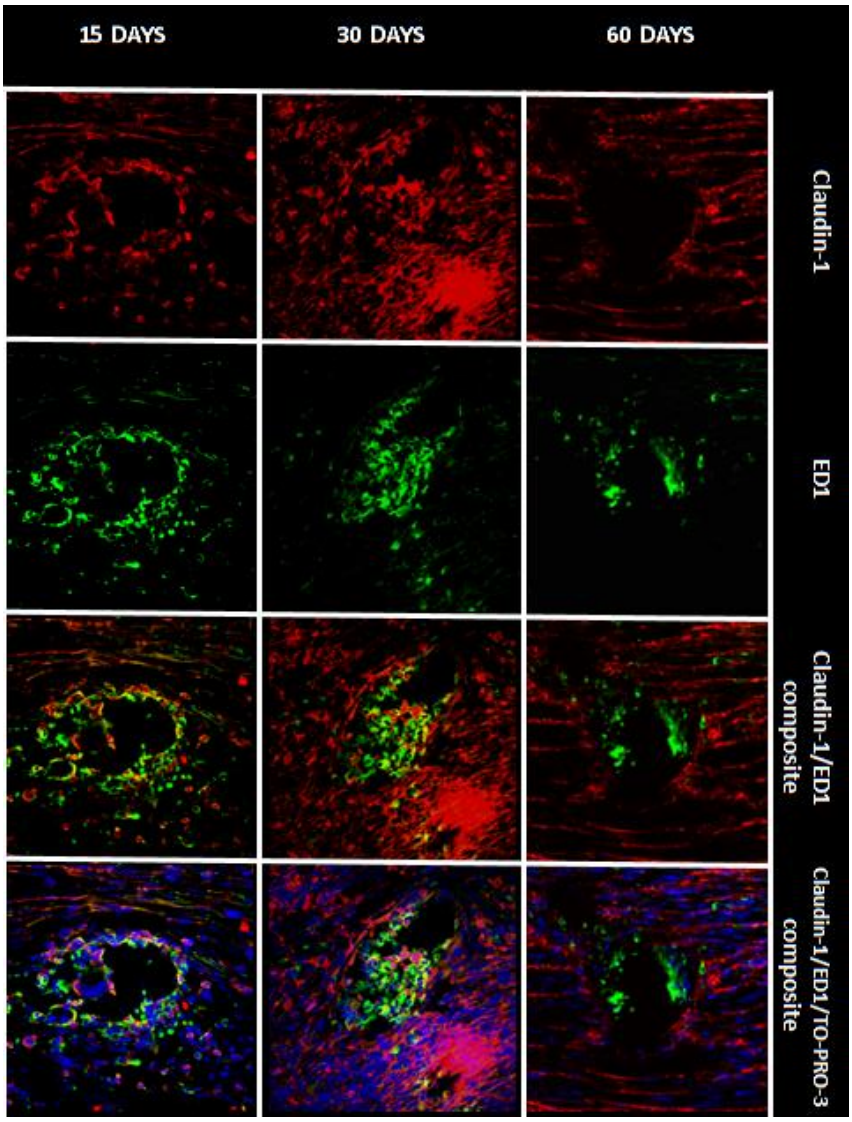

Figure 4-6 Immunolabeling nerve tissue with Claudin-1, ED1, and TO-PRO-3 of subchronic amputation model. Scale bar; 50 µm

Discussion

Acute amputation and subchronic amputation followed by a REMI implantation showed comparable results for the ED1 and Claudin-1 optical densitometry results, which support previous assertions that subchronic amputation does not significantly

affect the regenerative pattern observed in the peripheral nerve, despite of the difference in nerve regeneration extent as quantified in Chapter 4.

Perineurial cells and inherently TJ formation surrounding the scar has been suggested in this study as a plausible explanation for the long-term interfacing failure of multi-electrode arrays. As expected from previous results in chapter 2, the ED1 signal within the scar is significantly higher than outside of the scar, which further supports the concept that there is a clear immune response to the electrodes in the sciatic nerve. In quantitative terms, the gray (or optical densitometry) values for Claudin-1 revealed no significant differences between the inner scar region and the immediate external region of the scar for the acutely and subchronically amputated nerve samples. Nevertheless, a pattern for both amputation conditions was observed. At day 15, the optical densitometry values were higher within the scar than external to it. The optical densitometry values are approximately the same at day 30. At day 60, the optical densitometry values external to the scar region surpassed the values of those within the scar. This seems to indicate that initially, the TJs are abundant throughout the tissue sample, and as time progresses through the 30 and 60-day time points, the TJs become more concentrated outside of scar area. Qualitatively, the TJs seems to be forming among the (proposed forming) perineurial cells and sealing the scar as time progresses which could potentially lead to ion diffusion obstruction in the extracellular matrix and result in electrode interfacing failure. Perineurial recruitment along with TJ formation around the fibroblast and macrophage (Lefurge, Goodall et al. 1991) scar would directly hinder the ion influx into the ECM where the exposed tip of the REMI would be located. Figure 4-3 indicates that the TJs appear to be organizing and concentrating in relation to the region external of the scar. Gap junctions, which are intercellular channels, mediate the traffic of ions and a variety of molecular messengers between contiguous cells (Dezawa, Mutoh et al. 1998), are hypothesized to not have an effect in the ion influx in the extracellular matrix. Gap junctions connect the cytoplasm of two adjacent cells for communication and

transportation purposes; however, gap junctions do not aid in the diffusion rate or ion influx in the extracellular matrix, where the electrodes are found. Thus, formation of the BNB around the interfacing electrodes as the nerve regenerates may be a viable mechanism for the failure of such electrodes in the peripheral nervous system.

Chapter 5

Conclusion and Future Work

Neural prosthetics interfaced directly to the peripheral nervous system will, in the near future, assist amputees in performing quotidian activities with greater efficiency through the manipulation of dexterous upper limb prosthetics. Despite improvement in robotics and inherently in prosthetics, these devices are still limited by the lack of long-term interfacing reliability and specific degrees-of-freedom control, rendering them inadequate for clinical purposes. Interfacing of the central nervous system has been well documented to fail as a result of glial scar formation at the site of implantation (Polikov, Tresco et al. 2005); whereas the basis for peripheral interfacing failure remains an elusive subject.

This study had a dual purpose: to further explore the mechanisms for peripheral nervous interfacing failure and to evaluate the effect of a 30-day subchronic amputation followed by a REMI implantation. The inflammatory response to the iridium-platinum multi-electrode array was assessed. Previous electrophysiological recordings from our lab show a progressive increment in the percentage of active sites from the day of implant culminating at a maximum amount at day 21; subsequently, a decrease in percentage of active sites are seen until all the channels fail (figure 1-7). Histological results for acutely and subchronically amputated animals show a progressive decrease in the scar size from 15 to 60 days post REMI implantation. The direct correlation between scar size and percentage of active electrode channels does not fully account for the eventual electrode lead failure, which would lead one to discard the foreign body response as possible factor for action potential recording failure. However, despite the successive decrement in scar size at the three different time points, the distance and obstruction that the scar creates between electrode and action potential may still be significant in obtaining action potentials signals above noise levels.

Sciatic nerve regeneration through the REMI under acute amputation conditions has been shown to be progressive with remyelination of the axons taking place within approximately 20 days (Smith and Hall 1980). Under subchronic amputation conditions, the remyelination process is completed no earlier than 15 days, which resembles results for acute conditions in which peripheral axons were completely demyelinated using LPC followed by remyelination of the axons within 20 days (Smith and Hall 1980; Seifert, Desai et al. 2011). Further, the constant remyelination trend observed in Chapter 3 does not appear to be in full agreement with the electrophysiology observed by Khobragade's work in 2011. Before axons are myelinated, there is a block in conduction; however, the association of Schwann cells with unmyelinated axons will initiate conduction (Smith and Hall 1980). At 20 days, when remyelination has practically taken place and conduction of the axons is near pre-injury level, the highest percentage of active channels is also observed. In other words, there is an initial direct correlation between axon regrowth or remyelination and percentage of active electrode channels. After this direct correlation reaches a maximum at 21 days, active channel numbers declines while axon regrowth and remyelination continue to increase. At which point, the correlation between axon regrowth or remyelination and percentage of active channels becomes inverse. Thus, electrode failure must be the result of different underlying mechanism.

Here we have hypothesized that the BNB may play an underlying role in the decay in quality of the recorded signals. Tight junction formation and distribution in relation to the scar was studied to potentially understand how these TJs could affect the ion diffusion originating from the action potentials. If tight junctions among the axons, macrophages, or the scar as a whole become abundant enough it could form a barrier which would not allow the necessary diffusion rate of ions for the electrodes to properly work. Results indicate that TJs are initially distributed through the nerve regenerate, with a higher concentration of them within the scar area. Sixty days after REMI implantation, the concentration of TJs shifted towards the region external of the scar and allocated

themselves in a more structurally organized and discrete manner than previous time points.

Scar size, nerve regeneration, and remyelination do not play a major role in the failure of peripheral nerve interfacing; however, these processes may still be factors accountable for the pattern observed in signal recording. When the REMI is implanted post acute or subchronic amputation, the amount of channels able to record will be nonexistent due to the obvious lack of nerves found within the REMI and in proximity to the electrodes. Once the regenerate has bridged the gap between the proximal and distal stumps, two processes-- foreign body response and remyelination, which have been taking place--will now play a more direct role. The foreign body response will form a scar composed of macrophages and fibroblasts around the electrodes (Lefurge, Goodall et al. 1991), increasing the distance between the action potential and electrode, thus increasing impedance and partially preventing 100% of the channels recording any neural depolarization signals above noise. Simultaneously, remyelination is taking place, which will improve the conduction of the axons, allowing the electrodes to record this activity. After about 20 days, when remyelination has reached its peak and the scar size is decreasing, the high percentage of active channels are seen, meanwhile, TJs among the perineurial cells, which we have hypothesized take longer time to organize into an obstructive barrier. Albeit scar size decreasing (which even then will create distance between electrode and action potential) and axons being remyelinated, insulation of the electrode formed by the BNB could be the cause of long-term interfacing failure.

Acute amputation and subchronic amputation followed by a REMI implantation showed comparable results for the foreign body response and BNB formation. However, after 30 and 60 days the subchronic model showed to be significantly inferior in terms of axon regeneration and remyelination than the acute mode, despite both having models having near identical patterns. Nerve regeneration results from Chapter 3 appear to be

counter-intuitive because axon outgrowth has been proven to be enhanced by previous injury (McQuarrie and Grafstein 1973). This is of great clinical relevance because peripheral neural interfacing candidates would be required to be immediately interfaced following an amputation to obtain an ideal outcome.

Transgenic mice lacking genes for proper tight junctions have been studied for over 20 years, from which it has been established that claudins are the primary seal-forming proteins (Mitic, Van Itallie et al. 2000). Also, mannitol and Derp p 1 have been proven to disrupt TJs of the blood-brain barrier and endolethial cell (BBB), thus rendering these tissues permeable and allowing a higher degree of diffusion (Wan, Winton et al. 1999; Nagy, Pappius et al. 2004). Derp p1 accomplishes TJ disruption of such by cleavage of the TJ adhesion protein occluding (Wan, Winton et al. 1999). Mannitol manages to disrupt the overall integrity and impermeability properties of BBB due to the hyperosmotic conditions created by infusion of this sugar alcohol into the nerve (Nagy, Peters et al. 1984; Nagy, Pappius et al. 2004). Claudin-knowckout mice or TJ-disrupting solutions may be used to test the hypothesis that TJs formation among the cells in the regenerating nerve is responsible for long-term electrode failure. Claudin-1 deficient mice do not live longer than 1 day (Furuse, Hata et al. 2002), which does not make this a viable option. Thus, the use of transgenic mice may be extreme and illicit unfavorable conditions for proper experimentation on the animals. Rather, infusions of TJ proteolytic or hyperosmotic solutions could be administered to the specific site of interest to directly test effects of impermeability around the interfacing electrodes while avoiding secondary effects on the animals such as diminished life span. Future experiments should focus on the integrity and possible formation of the BNB around the interfacing electrodes, more specifically, the tight junctions, as the leading cause of peripheral nervous system interfacing failure.

References

Akassoglou, K., W. M. Yu, et al. (2002). "Fibrin inhibits peripheral nerve remyelination by regulating Schwann cell differentiation." Neuron **33**(6): 861-875.

Anderson, J. M., A. Rodriguez, et al. (2008). Foreign body reaction to biomaterials. Seminars in immunology, NIH Public Access.

Biran, R., D. C. Martin, et al. (2005). "Neuronal cell loss accompanies the brain tissue response to chronically implanted silicon microelectrode arrays." Experimental neurology **195**(1): 115-126.

Bogue, R. (2009). "Exoskeletons and robotic prosthetics: a review of recent developments." Industrial Robot: An International Journal **36**(5): 421-427.

Bossi, S., A. Benvenuto, et al. (2010). Preliminary investigations on laminin coatings for flexible polyimide/platinum thin films for PNS applications, IEEE.

Bowman, B. R. and R. C. Erickson (1985). "Acute and chronic implantation of coiled wire intraneural electrodes during cyclical electrical stimulation." Annals of biomedical engineering **13**(1): 75-93.

Branner, A. and R. A. Normann (2000). "A multielectrode array for intrafascicular recording and stimulation in sciatic nerve of cats." Brain research bulletin **51**(4): 293-306.

Branner, A., R. B. Stein, et al. (2004). "Long-term stimulation and recording with a penetrating microelectrode array in cat sciatic nerve." Biomedical Engineering, IEEE Transactions on **51**(1): 146-157.

Branner, A., R. B. Stein, et al. (2001). "Selective stimulation of cat sciatic nerve using an array of varying-length microelectrodes." Journal of neurophysiology **85**(4): 1585-1594.

Brown, P. B., H. R. Koerber, et al. (2004). "From innervation density to tactile acuity: 1. Spatial representation." Brain research **1011**(1): 14-32.

Carlson, J., A. C. Lais, et al. (1979). "Axonal atrophy from permanent peripheral axotomy in adult cat." Journal of Neuropathology & Experimental Neurology **38**(6): 579-585.

Carter, R. R. and J. C. Houk (1993). "Multiple single-unit recordings from the CNS using thin-film electrode arrays." Rehabilitation Engineering, IEEE Transactions on **1**(3): 175-184.

Coates, S. D. (2008). "Neural Interfacing: Forging the Human-Machine Connection." Synthesis Lectures on Biomedical Engineering **3**(1): 1-112.

Coleman, D., R. King, et al. (2004). "The foreign body reaction: a chronic inflammatory response." Journal of biomedical materials research **8**(5): 199-211.

Darian-Smith, C. and C. D. Gilbert (1994). "Axonal sprouting accompanies functional reorganization in adult cat striate cortex." Nature **368**(6473): 737-740.

Davis, L., T. Gordon, et al. (1978). "Compound action potentials recorded from mammalian peripheral nerves following ligation or resuturing." The Journal of physiology **285**(1): 543-559.

Dezawa, M., T. Mutoh, et al. (1998). "Putative gap junctional communication between axon and regenerating Schwann cells during mammalian peripheral nerve regeneration." Neuroscience **85**(3): 663-667.

Dhillon, G. S., S. M. Lawrence, et al. (2004). "Residual function in peripheral nerve stumps of amputees: implications for neural control of artificial limbs." The Journal of hand surgery **29**(4): 605-615.
Di Lullo, G. A., S. M. Sweeney, et al. (2002). "Mapping the ligand-binding sites and disease-associated mutations on the most abundant protein in the human, type I collagen." Journal of Biological Chemistry **277**(6): 4223-4231.
Dijkstra, C., E. Döpp, et al. (1985). "The heterogeneity of mononuclear phagocytes in lymphoid organs: distinct macrophage subpopulations in the rat recognized by monoclonal antibodies ED1, ED2 and ED3." Immunology **54**(3): 589.
Donnerer, J. (2003). "Regeneration of primary sensory neurons." Pharmacology **67**(4): 169-181.
Durand, D., H. Park, et al. (2009). Models of the peripheral nerves for detection and control of neural activity, IEEE.
Eaton, K. P. and C. S. Henriquez (2005). "Confounded spikes generated by synchrony within neural tissue models." Neurocomputing **65**: 851-857.
Edell, D. J., V. Toi, et al. (1992). "Factors influencing the biocompatibility of insertable silicon microshafts in cerebral cortex." Biomedical Engineering, IEEE Transactions on **39**(6): 635-643.
Faweett, J. and R. J. Keynes (1990). "Peripheral nerve regeneration." Annual review of neuroscience **13**(1): 43-60.
Fenrich, K. and T. Gordon (2003). "Canadian Association of Neuroscience review: axonal regeneration in the peripheral and central nervous systems-current issues and advances." The Canadian Journal of Neurological Sciences **31**(2): 142-156.
Fisher, L., D. Tyler, et al. (2009). "Chronic stability and selectivity of four-contact spiral nerve-cuff electrodes in stimulating the human femoral nerve." Journal of neural engineering **6**(4): 046010.
FitzGerald, J. J., N. Lago, et al. (2012). "A regenerative microchannel neural interface for recording from and stimulating peripheral axons in vivo." Journal of neural engineering **9**: 016010.
Fu, S. Y. and T. Gordon (1997). "The cellular and molecular basis of peripheral nerve regeneration." Molecular neurobiology **14**(1): 67-116.
Furuse, M., M. Hata, et al. (2002). "Claudin-based tight junctions are crucial for the mammalian epidermal barrier a lesson from claudin-1–deficient mice." The Journal of cell biology **156**(6): 1099-1111.
Garde, K., E. Keefer, et al. (2009). "Early interfaced neural activity from chronic amputated nerves." Frontiers in Neuroengineering **2**.
Goodall, E. V. and K. Horch (1992). "Separation of action potentials in multiunit intrafascicular recordings." Biomedical Engineering, IEEE Transactions on **39**(3): 289-295.
Goodall, E. V., T. Lefurge, et al. (1991). "Information contained in sensory nerve recordings made with intrafascicular electrodes." Biomedical Engineering, IEEE Transactions on **38**(9): 846-850.
Green, R. A., N. H. Lovell, et al. (2008). "Conducting polymers for neural interfaces: challenges in developing an effective long-term implant." Biomaterials **29**(24): 3393-3399.

He, W. and R. V. Bellamkonda (2005). "Nanoscale neuro-integrative coatings for neural implants." Biomaterials **26**(16): 2983-2990.
He, W., G. C. McConnell, et al. (2006). "Nanoscale laminin coating modulates cortical scarring response around implanted silicon microelectrode arrays." Journal of neural engineering **3**(4): 316.
Heath, C. A. and G. E. Rutkowski (1998). "The development of bioartificial nerve grafts for peripheral-nerve regeneration." Trends in biotechnology **16**(4): 163-168.
Hoffer, J., R. Stein, et al. (1979). "Differential atrophy of sensory and motor fibers following section of cat peripheral nerves." Brain research **178**(2): 347-361.
Horner, P. J. and F. H. Gage (2000). "Regenerating the damaged central nervous system." NATURE-LONDON-: 963-970.
Huebsch, N. and D. J. Mooney (2009). "Inspiration and application in the evolution of biomaterials." Nature **462**(7272): 426-432.
Ignatius, M., N. Sawhney, et al. (1998). "Bioactive surface coatings for nanoscale instruments: effects on CNS neurons." Journal of biomedical materials research **40**(2): 264-274.
Ismagilov, R. F. (2003). "Integrated microfluidic systems." Angewandte Chemie International Edition **42**(35): 4130-4132.
Jan, E., J. L. Hendricks, et al. (2009). "Layered carbon nanotube-polyelectrolyte electrodes outperform traditional neural interface materials." Nano letters **9**(12): 4012-4018.
Karami, G., K. Ahmadi, et al. (2012). "Better Mental Component of Quality of Life in Amputee." Iranian J Publ Health **41**(7).
Kashiwamura, Y., Y. Sano, et al. (2011). "Hydrocortisone enhances the function of the blood-nerve barrier through the up-regulation of claudin-5." Neurochemical research **36**(5): 849-855.
Kawamura, Y. and P. J. Dyck (1981). "Permanent axotomy by amputation results in loss of motor neurons in man." Journal of Neuropathology & Experimental Neurology **40**(6): 658-666.
Keefer, E. W., B. R. Botterman, et al. (2008). "Carbon nanotube coating improves neuronal recordings." Nature nanotechnology **3**(7): 434-439.
Keilhoff, G., F. Stang, et al. (2003). "Bio-compatibility of type I/III collagen matrix for peripheral nerve reconstruction." Biomaterials **24**(16): 2779-2787.
Khobragade, N. (2011). "Micromotion and Scarring Do Not Contribue to the Failure of Regenerative Peipheral Neural Interfacing." (1): 67.
Khobragrade, N. (2011). "Micromotion and Scarring do not Lead to Failure of Peripheral Neural Interfacing ".
Kim, Y. and M. I. Romero-Ortega (2012). "Material considerations for peripheral nerve interfacing." MRS bulletin **37**(06): 573-580.
Krombach, F., S. Münzing, et al. (1997). "Cell size of alveolar macrophages: an interspecies comparison." Environmental health perspectives **105**(Suppl 5): 1261.
Lawrence, S. M., G. Dhillon, et al. (2004). "Acute peripheral nerve recording characteristics of polymer-based longitudinal intrafascicular electrodes." Neural Systems and Rehabilitation Engineering, IEEE Transactions on **12**(3): 345-348.

Lee, S. H., G. E. Carvell, et al. (2008). "Motor modulation of afferent somatosensory circuits." Nature neuroscience **11**(12): 1430-1438.
Lefurge, T., E. Goodall, et al. (1991). "Chronically implanted intrafascicular recording electrodes." Annals of biomedical engineering **19**(2): 197-207.
Leon, S., Y. Yin, et al. (2000). "Lens injury stimulates axon regeneration in the mature rat optic nerve." The Journal of neuroscience **20**(12): 4615-4626.
Liberson WT, H. H., Scott D, Dow A (1961). "Functional electrotherapy: stimulation of the peroneal nerve synchronized with the swing phase of hemiplegic patients." Arch Phys Med Rehabi **42**: 1010-1105.
Lindsay, R. M. (1988). "Nerve growth factors (NGF, BDNF) enhance axonal regeneration but are not required for survival of adult sensory neurons." The Journal of neuroscience **8**(7): 2394-2405.
Liu, T., J. D. Houle, et al. (2012). "Nanofibrous collagen nerve conduits for spinal cord repair." Tissue Engineering Part A **18**(9-10): 1057-1066.
Liu, X., D. B. McCreery, et al. (1999). "Stability of the interface between neural tissue and chronically implanted intracortical microelectrodes." Rehabilitation Engineering, IEEE Transactions on **7**(3): 315-326.
Loeb, G. and R. Peck (1996). "Cuff electrodes for chronic stimulation and recording of peripheral nerve activity." Journal of neuroscience methods **64**(1): 95-103.
Lotfi, P. and M. Romero-Ortega (2011). Control of neural interfacing in peripheral nerves through regenerative molecular guidance, IEEE.
Mamedov, A. A., N. A. Kotov, et al. (2002). "Molecular design of strong single-wall carbon nanotube/polyelectrolyte multilayer composites." Nature Materials **1**(3): 190-194.
McFarland, D. J., W. A. Sarnacki, et al. (2010). "IOPscience-Electroencephalographic (EEG) control of three-dimensional movement." Journal of neural engineering **7**: 036007.
McNaughton, T. G. and K. W. Horch (1996). "Metallized polymer fibers as leadwires and intrafascicular microelectrodes." Journal of neuroscience methods **70**(1): 103-107.
McQuarrie, I. G. and B. Grafstein (1973). "Axon outgrowth enhanced by a previous nerve injury." Archives of Neurology **29**(1): 53.
Merrill, D. R., M. Bikson, et al. (2005). "Electrical stimulation of excitable tissue: design of efficacious and safe protocols." Journal of neuroscience methods **141**(2): 171-198.
Merrill, D. R. and P. A. Tresco (2005). "Impedance characterization of microarray recording electrodes in vitro." Biomedical Engineering, IEEE Transactions on **52**(11): 1960-1965.
Miller, L. A., R. D. Lipschutz, et al. (2008). "Control of a six degree of freedom prosthetic arm after targeted muscle reinnervation surgery." Archives of physical medicine and rehabilitation **89**(11): 2057-2065.
Mitic, L. L., C. M. Van Itallie, et al. (2000). "Molecular physiology and pathophysiology of tight junctions I. Tight junction structure and function: lessons from mutant animals and proteins." American Journal of Physiology-Gastrointestinal and Liver Physiology **279**(2): G250-G254.

Nagy, Z., H. M. Pappius, et al. (2004). "Opening of tight junctions in cerebral endothelium. I. Effect of hyperosmolar mannitol infused through the internal carotid artery." The Journal of comparative neurology **185**(3): 569-578.
Nagy, Z., H. Peters, et al. (1984). "Fracture faces of cell junctions in cerebral endothelium during normal and hyperosmotic conditions." Laboratory investigation; a journal of technical methods and pathology **50**(3): 313.
Navarro, X., T. B. Krueger, et al. (2005). "A critical review of interfaces with the peripheral nervous system for the control of neuroprostheses and hybrid bionic systems." Journal of the Peripheral Nervous System **10**(3): 229-258.
Navarro, X., M. Vivó, et al. (2007). "Neural plasticity after peripheral nerve injury and regeneration." Progress in neurobiology **82**(4): 163.
Poduslo, J. F., G. L. Curran, et al. (1994). "Macromolecular permeability across the blood-nerve and blood-brain barriers." Proceedings of the National Academy of Sciences **91**(12): 5705-5709.
Poliak, S., S. Matlis, et al. (2002). "Distinct claudins and associated PDZ proteins form different autotypic tight junctions in myelinating Schwann cells." The Journal of cell biology **159**(2): 361-372.
Polikov, V. S., P. A. Tresco, et al. (2005). "Response of brain tissue to chronically implanted neural electrodes." Journal of neuroscience methods **148**(1): 1-18.
Porter, R., W. Adey, et al. (1964). "Measurement of electrical impedance in the human brain Some preliminary observations." Neurology **14**(11): 1002-1012.
Pummi, K. P., A. M. Heape, et al. (2004). "Tight junction proteins ZO-1, occludin, and claudins in developing and adult human perineurium." Journal of Histochemistry & Cytochemistry **52**(8): 1037-1046.
Rechthand, E. and S. I. Rapoport (1987). "Regulation of the microenvironment of peripheral nerve: role of the blood-nerve barrier." Progress in neurobiology **28**(4): 303.
Resnik, L., M. R. Meucci, et al. (2012). "Advanced upper limb prosthetic devices: implications for upper limb prosthetic rehabilitation." Archives of physical medicine and rehabilitation **93**(4): 710-717.
Rosengren, A., N. Danielsen, et al. (1999). "Reactive capsule formation around soft-tissue implants is related to cell necrosis." Journal of biomedical materials research **46**(4): 458-464.
Salcman, M. and M. J. Bak (1976). "A new chronic recording intracortical microelectrode." Medical and Biological Engineering and Computing **14**(1): 42-50.
Schwartz, A. B., X. T. Cui, et al. (2006). "Brain-controlled interfaces: movement restoration with neural prosthetics." Neuron **52**(1): 205-220.
Seifert, J., V. Desai, et al. (2011). "Normal Molecular Repair Mechanisms in Regenerative Peripheral Nerve Interfaces Allow Recording of Early Spike Activity Despite Immature Myelination." Neural Systems and Rehabilitation Engineering, IEEE Transactions on(99): 1-1.
Shoham, S. (2001). Advances towards an implantable motor cortical interface, The University of Utah.
Smith, K. and S. Hall (1980). "Nerve conduction during peripheral demyelination and remyelination." Journal of the neurological sciences **48**(2): 201-219.

Stieglitz, T., H. Beutel, et al. (2000). "Micromachined, polyimide-based devices for flexible neural interfaces." Biomedical Microdevices **2**(4): 283-294.
Szarowski, D., M. Andersen, et al. (2003). "Brain responses to micro-machined silicon devices." Brain research **983**(1): 23-35.
Taylor, A. S., A. D. Cunningham, et al. (1999). Board-to-board connector assembly, Google Patents.
Terenghi, G. (2002). "Peripheral nerve regeneration and neurotrophic factors." Journal of anatomy **194**(1): 1-14.
Thoma, H., W. Girsch, et al. (1989). "Technology and long-term application of an epineural electrode." ASAIO transactions/American Society for Artificial Internal Organs **35**(3): 490.
Tornqvist, E. and H. Aldskogius (1994). "Motoneuron survival is not affected by the proximo-distal level of axotomy but by the possibility of regenerating axons to gain access to the distal nerve stump." Journal of neuroscience research **39**(2): 159-165.
Turner, A., N. Dowell, et al. (2000). "Attachment of astroglial cells to microfabricated pillar arrays of different geometries." Journal of biomedical materials research **51**(3): 430-441.
Tyler, D. J. and D. M. Durand (1997). "A slowly penetrating interfascicular nerve electrode for selective activation of peripheral nerves." Rehabilitation Engineering, IEEE Transactions on **5**(1): 51-61.
Vaughan, T. M. (2003). "Guest editorial brain-computer interface technology: a review of the second international meeting." Neural Systems and Rehabilitation Engineering, IEEE Transactions on **11**(2): 94-109.
Velliste, M., S. Perel, et al. (2008). "Cortical control of a prosthetic arm for self-feeding." Nature **453**(7198): 1098-1101.
Venkatraman, S., K. Elkabany, et al. (2009). "A system for neural recording and closed-loop intracortical microstimulation in awake rodents." Biomedical Engineering, IEEE Transactions on **56**(1): 15-22.
Viswanathan, V. and S. Kumpatla (2011). "Pattern and Causes of Amputation in Diabetic Patients–A Multicentric Study from India." Journal of association of physicians of India **59**: 148-1451.
Wallman, L., Y. Zhang, et al. (2001). "The geometric design of micromachined silicon sieve electrodes influences functional nerve regeneration." Biomaterials **22**(10): 1187-1193.
Wan, H., H. L. Winton, et al. (1999). "Der p 1 facilitates transepithelial allergen delivery by disruption of tight junctions." Journal of Clinical Investigation **104**: 123-133.
Warwick, K., M. Gasson, et al. (2003). "The application of implant technology for cybernetic systems." Archives of Neurology **60**(10): 1369.
Watson, C. (2012). Investigations Into Causes of Failure of Regenerative Peripheral Nerve Interfaces.
Weiland, J. D. and D. J. Anderson (2000). "Chronic neural stimulation with thin-film, iridium oxide electrodes." Biomedical Engineering, IEEE Transactions on **47**(7): 911-918.

Weir, S., P. Ephraim, et al. (2010). "Effects of paediatric limb loss on healthcare utilisation, schooling and parental labour supply." Disability & Rehabilitation **32**(24): 2046-2055.

Winter, J. O., S. F. Cogan, et al. (2007). "Neurotrophin-eluting hydrogel coatings for neural stimulating electrodes." Journal of Biomedical Materials Research Part B: Applied Biomaterials **81**(2): 551-563.

Wong, B. and D. Mattox (1991). "Experimental nerve regeneration. A review." Otolaryngologic clinics of North America **24**(3): 739.

Yoo, J. M., A. Sharma, et al. (2012). "Excimer-laser deinsulation of Parylene-C coated Utah electrode array tips." Sensors and Actuators B: Chemical.

Yucel, D., G. T. Kose, et al. (2010). "Polyester based nerve guidance conduit design." Biomaterials **31**(7): 1596-1603.

Zarbin, M. A., C. Montemagno, et al. (2012). "Regenerative nanomedicine and the treatment of degenerative retinal diseases." Wiley Interdisciplinary Reviews: Nanomedicine and Nanobiotechnology **4**(1): 113-137.

Zhao, Q., J. Drott, et al. (1997). "Rat sciatic nerve regeneration through a micromachined silicon chip." Biomaterials **18**(1): 75-80.

Ziegler-Graham, K., E. J. MacKenzie, et al. (2008). "Estimating the prevalence of limb loss in the United States: 2005 to 2050." Arch Phys Med Rehabil **89**(3): 422-429.

Biographical Information

Camilo Andres Sanchez Useche was born of Gustavo Sanchez Susunaga and Liliana Useche Martinez on April 9th 1988 in Ibague, Colombia. Camilo and his family moved to Fort Worth, Texas in 1999, where he was enrolled in the public education system. Inspired by science fiction and motivated by the drive to help the disabled, his junior year in high school Camilo set himself to one day work in neuroprosthetics. In August 2011 Dr. Romero granted him the opportunity to work in a neuroprosthetic-related laboratory, where Camilo opted to challenge himself and completed a thesis by November 2012. Camilo plans on contributing to reach a day where amputees, paraplegics, and quadriplegics will be able to physically interact with their environment without any limitations.